ACS OMEGA

Open Access

http://pubs.acs.org/journal/acsodf

Article

Automated Generation of a Compact Chemical Kinetic Model for *n*-Pentane Combustion

Venus Amiri, Rubik Asatryan, and Mark Swihart*

Cite This: *ACS Omega* 2023, 8, 49098−49114

Read Online

ACCESS | Metrics & More | Article Recommendations | Supporting Information

ABSTRACT: We have employed automated mechanism generation tools to construct a detailed chemical kinetic model for combustion of *n*-pentane, as a step toward the generation of compact kinetic models for larger alkanes. Pentane is of particular interest as a prototype for combustion of alkanes and as the smallest paraffin employed as a hybrid rocket fuel, albeit at cryogenic conditions. A reaction mechanism for pentane combustion thus provides a foundation for modeling combustion of extra-large alkanes (paraffins) that are of more practical interest as hybrid rocket fuels, for which manual construction becomes infeasible. Here, an *n*-pentane combustion kinetic model is developed using the open-source software package Reaction Mechanism Generator (RMG). The model was generated and tested across a range of temperatures (650 to 1350 K) and equivalence ratios (0.5, 1.0, 2.0) at pressures of 1 and 10 atm. Available thermodynamic and kinetic databases were incorporated wherever possible. Predictions using the mechanism were validated against the published laminar burning velocities (S_u) and ignition delay times (IDT) of *n*-pentane. To improve the model performance, a comprehensive analysis, including reaction path and sensitivity analyses of *n*-pentane oxidation, was performed, leading us to modify the thermochemistry and rate parameters for a few key species and reactions. These were combined as a separate data set, an RMG library, that was then used during mechanism generation. The resulting model predicted IDTs as accurately as the best manually constructed mechanisms, while remaining much more compact. It predicted flame speeds to within 10% of published experimental results. The degree of success of automated mechanism generation for this case suggests that it can be extended to construct reliable and compact models for combustion of larger *n*-alkanes, particularly when using this mechanism as a seed submodel.

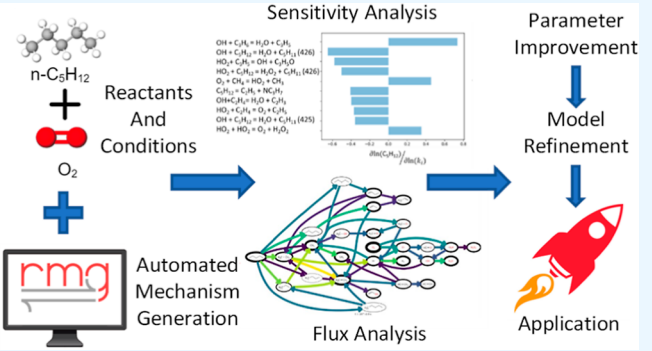

1. INTRODUCTION

Detailed kinetic models of combustion processes include complex pressure- and temperature- dependent free-radical reactions among numerous reaction intermediates. These processes must be coupled to mass transfer, heat transfer, and thermodynamic constraints to model combustion processes. Recent advances in numerical solvers and computational chemistry methods allow the direct use of detailed kinetic models without dramatic simplifications, including all of the elementary processes that can occur, at least for simple flow fields and flame structures. Paraffin wax hybrid rocket fuels (HRFs) include alkane molecules with 30−50 carbon atoms.[1] Generating mechanisms for such large molecules is challenging due to the dramatic increase in the number of relevant chemical species and elementary reactions with fuel size. Construction of mechanisms for such large molecules can potentially be facilitated by automated tools.

Paraffin wax is an advanced fuel for hybrid rocket propulsion, exhibiting higher regression and burning rates (increased thrust) compared to conventional fuels.[2−4] It is also safer and more environmentally benign than conventional HRFs. Understanding the mechanism of combustion and pyrolysis of paraffin wax is important for further improvement of the rocket performance. Pentane was the first paraffinic HRF, used as a solid under cryogenic conditions by US Army researchers.[5,6] Oxidation of *n*-pentane has been widely studied by experiment, theory, and modeling. General features of product distributions and its combustion characteristics have been widely reported.[7−18] As the smallest relevant paraffin, *n*-pentane serves as an ideal model for computational kinetics of combustion of paraffin wax, as well as soot formation (via, particularly, generation of cyclopentadiene derivatives[19]), though we do not address soot formation here. Degradation and oxidation pathways for larger *n*-alkanes are expected to mirror those identified for pentane combustion.[11−18] Specifically, *n*-pentane oxidation allows consideration of all relevant

Received: September 15, 2023
Revised: November 21, 2023
Accepted: November 24, 2023
Published: December 14, 2023

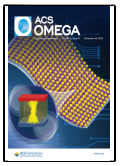

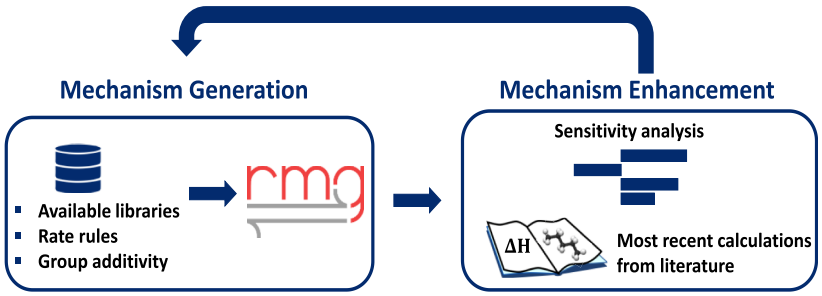

Figure 1. Schematic illustration of the model development and refinement.

intramolecular H-migration reactions, which are important for modeling low-temperature combustion and ignition.[11−13,20−28] The proximity of the outermost secondary carbons in *n*-pentane enables the inclusion of isomerization reactions of oxygen-centered RO_2 and O_2QOOH intermediate radicals between C_2 and C_4 (and any other secondary β-centered) carbon atoms of larger *n*-alkanes. Such reactions play key roles at low flame temperatures. Note that the low temperature chemistry is still an area of some uncertainty, and new developments are underway.

Detailed chemical kinetic models typically involve hundreds of species (reaction intermediates) and thousands of elementary reactions. Several automated tools have been developed and published, including Reaction Mechanism Generator (RMG), EXGAS, REACTION, NetGen, and MAMOX, to facilitate this tedious and error-prone process.[29−32] RMG is an open-source software package developed by Green and co-workers (MIT and Northeastern University groups). RMG builds kinetic models based on libraries of known reactions and their kinetics, generalized chemical knowledge, rate rules, and group additivity (GA) methods.[33] It uses a rate-based algorithm to specify which species and reactions are included in the model. Chemical species, and the reactions among them, are added until the rate of production of all species falls below a prespecified termination criterion. Species thermochemistry and reaction rate parameters are selected from a hierarchy of sources, starting from experimental values in libraries and using GA and rate rules to estimate rates when no other data is available. RMG is one of the most advanced and widely used software packages in the field. It also offers a stable, robust programming architecture to develop extensible and modular code. Here, we used RMG as the primary tool to facilitate the generation of detailed kinetic models. The overall goal of this study was to use automated mechanism generation as a tool to develop a detailed kinetic mechanism for *n*-pentane combustion that was significantly more compact (many fewer species) than the best published mechanisms while providing similarly accurate predictions of ignition delay time (IDT) and flame speed over a broad range of conditions.

In future studies, we can then employ this *n*-pentane combustion mechanism as a submechanism (seed) in the context of predicting global combustion characteristics for large and extra-large hydrocarbons, including paraffin wax HRFs.

Several reaction mechanisms involving midsized alkanes have been generated using RMG, mainly relying on generated basic alkane models with added cross reactions, such as that for pentane + NO_2.[36] A more recent detailed model has been developed for combustion of alkenes.[37] However, the automatically generated models may not yet match the performance of the manually constructed and tuned reaction models. Therefore, analyzing the applicability of the automatically generated models for well-studied systems and assessing the potential of these approaches for creating submodels to be kept fixed and used as "seeds" for constructing larger mechanisms remains valuable. In addition, the extension of the specific built-in libraries for large *n*-paraffins would be an advantage for future model developments. Thus, pentane combustion was the focus of this study.

2. CHEMICAL KINETIC MODEL DEVELOPMENT

RMG was used to generate a gas-phase reaction mechanism including both thermochemical and reaction rate parameters taken from selected libraries that include the most recent theoretically based and experimental data, supplemented with estimates based upon GA and rate rules,[33] as shown schematically in Figure 1. Mechanism generation was performed with all relevant reaction families by default. The final termination criterion for simulations used in mechanism generation was 50% conversion of O_2, to keep the initial *n*-alkane as a major constituent throughout the generation conditions. Three parameters, temperature (T), pressure (P), and equivalence ratio (ϕ), were varied during mechanism generation. Generally, there are two main approaches to spanning a range of reaction conditions during mechanism generation. One can generate mechanisms separately, at different conditions, and then merge them, or one can employ a range of conditions during a single simulation. In the merged approach, we have generated a mechanism for each of the preselected temperatures individually (750, 950, 1150, 1350 K) at a single pressure and equivalence ratio. The generated mechanisms were combined to yield the final merged mechanism. This method would have to be repeated multiple times for different pressures, temperatures, and equivalence ratios to cover a wide range of conditions. For example, repeating these 4 temperatures at 3 values of equivalence ratio and 3 pressures would require merging 36 mechanisms from 36 sets of conditions. In the alternative, so-called ranged approach, the reaction conditions are sampled from a defined range of conditions.[33,37,38] In this range-based approach, instead of simulating a reactor for a fixed set of initial conditions, various conditions are selected from a specified parameter range by a weighted stochastic grid-sampling algorithm. The pseudorandomly sampled numbers are seeded, ensuring that the algorithm is deterministic. This provides a much more efficient route to generating a mechanism that is applicable across a range of conditions. Thus, throughout most of this study, we have used the ranged approach in RMG to simultaneously consider multiple reaction conditions spanning

https://doi.org/10.1021/acsomega.3c07079
ACS Omega 2023, 8, 49098−49114

a range of T, P, and ϕ. Some iterative refinement of mechanisms constructed by RMG is always required, as demonstrated in this study in full accord with results of Pio et al.[37] for gas-phase systems and Kreitz et al.[38] for heterogeneous catalysis. A summary of RMG settings is provided in Table S3, indicating the tolerances for the final model.

We used the manually constructed model of the National University of Ireland, Galway (NUIG), for combustion of pentane isomers, as a benchmark for comparison with experimental as well as simulation results.[15] The NUIG kinetic model has been tested and validated using rapid compression machine (RCM) results from NUIG and shock tube (ST) results from NUIG and Texas A&M University (TAMU).[15,16] We used ANSYS Chemkin-Pro 2023[39] to carry out ignition delay calculations for a homogeneous constant-pressure batch reactor, taking the IDT to be the time required for the temperature to increase by 400 K.

Our approach to automated generation of a mechanism for *n*-pentane oxidation was to draw on experimentally verified and first-principles-based data sources to the greatest extent possible while using rate-based criteria for growing the mechanism. The rate-based approach avoids the inclusion of species that are ultimately not important, in contrast to manual reaction mechanism construction methods in which we typically write all possible species generated by specific reaction types or rely on chemical intuition to select among them. This approach aims to generate both comprehensive and compact models. We thus employed a few reaction and thermochemistry libraries included with RMG, primarily involving data for small species chemistry. Specifically, the Burke submodel for H_2 combustion at high-pressures,[40] and the Klippenstein−Glarborg model based on the recent mechanism by Hashemi et al. for high-pressure methane combustion,[41] were utilized as sources of H_2/O_2 and C_1-C_2 chemistry, respectively. We also included updated thermochemistry databases available in the RMG for C_3-C_4 species. The thermochemistry was from a database by Goldsmith et al.[42] based on density functional theory (DFT) calculated geometries and refined QCISD(T) energies for a large number of combustion-relevant small species ("DFT_QCI_thermo"), as well as CBS-QB3 ("CBS_QB3_1dHR") and G4MP2 composite level predictions reported below.

The detailed and well-validated manually developed mechanism by Curran and co-workers implemented in RMG as CurranPentane library (abbreviated as CPL here) is well suited as a source of thermochemical and rate parameters for pentane combustion, from which a subset of species and reactions will be required during automated generation.[15] However, the full mechanism itself is rather large (675 species and 3065 reactions) and thus is not well-suited to serve as a seed mechanism for generation of combustion and pyrolysis models of larger paraffins while maintaining a tractable mechanism size.

Thus, C_5-chemistry, where possible, was drawn from CPL, which is based on the NUIG mechanism developed by Bugler et al.[15] RMG includes CPL as a source for both thermochemistry (primarily for C_5 and some C_4 species) and reaction kinetics of pentane isomers. Taking into account that a large portion of these data are generated using a GA method (primarily via the THERM[43] code and updated group values), and rate rule approximations, we have prioritized other data sets that are either based on first-principles calculations or obtained experimentally (see also Supporting Information).

In addition, in this study, we created a separate library for RMG to complement the built-in libraries and update key thermochemical and kinetic parameters, as described below. In this library, we particularly included the new results for thermochemistry of all nine isomers of C_5H_9 key radicals calculated by G4MP2 composite method as implemented in Gaussian 16[44] employing the ARM-2 atomization approach[45], as well as alternative kinetics data from the literature (vide infra) which will be discussed in Section 3.3. We have modified the most influential reaction parameters identified by sensitivity analysis and by analysis of the collision rate-violating reactions using alternative data within the uncertainty ranges of the estimated parameters to obtain more consistency with experiment (primarily IDTs and flame speeds).

To summarize, we employed three model development approaches based on the type of model generation (merged or ranged) and input data sets: (i) using fully estimated data with no built-in library (PN-ES), (ii) based on a single library, the CurranPentane library (PN-CPL), and (iii) using multiple libraries denoted as PN-ML, to invoke as many experimental and first-principles-based thermochemical and kinetic data as possible. The final mechanism that includes our own database (RMG-library), as introduced above and described further below, is denoted as PN-ML-m, where m denotes modified thermochemistry and rate parameters.

3. RESULTS AND DISCUSSION

3.1. Effects of Model Generation Approach and Employed Data Sets. A comparison of different utilized databases is presented in Figure 2, where PN stands for pentane. They were compared against three results from the literature, from both experiment and simulation. The approach spans not only the temperature range from 750 to 1350 K but also a pressure range from 1 to 10 atm and equivalence ratios from 0.5 to 2.0. Merging mechanism generated over this full

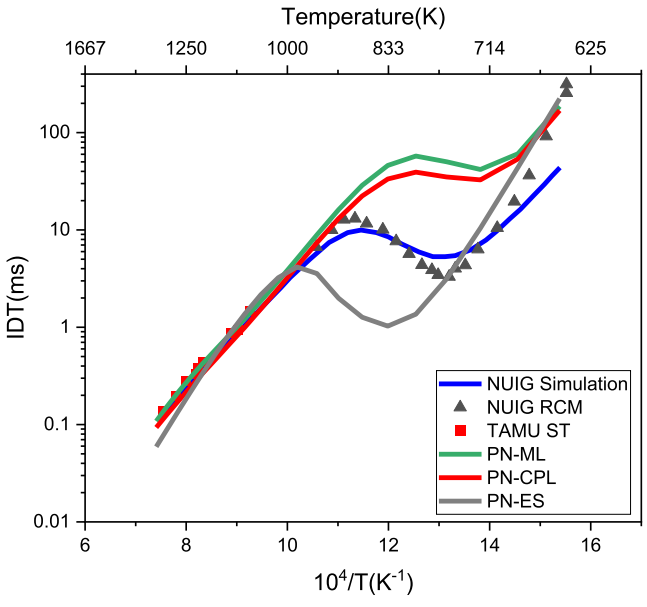

Figure 2. Effect of the use of thermochemical and kinetic libraries on model performance for $\phi = 2$ and $P = 10$ atm: using no libraries, only estimation methods (PN-ES), using only the Curran Pentane Library (PN-CPL), and employing higher fidelity data via multiple libraries. Symbols are experimental data; lines are model predictions.

https://doi.org/10.1021/acsomega.3c07079
ACS Omega 2023, 8, 49098−49114

space of T, P, and ϕ would further increase the size of the mechanism and is a less efficient approach to sampling that space than the ranged method.[46] Figure S1 shows the comparison of different merged approaches and the size changes of mechanism in Table S1. Therefore, unless otherwise specified, the ranged method was used throughout the remainder of the article and is not explicitly noted in figure legends and captions.

Using the ranged approach, we next tested the effect of employing thermochemical and rate parameters from available libraries on model performance. Initially, a more straightforward version of the kinetic model was developed exclusively based on the RMG-estimated parameters (a model constructed "from scratch", denoted as PN-ES) with no libraries included during model generation. This provides a baseline for automated generation with no information beyond GA predictions of thermochemistry and rate rules for kinetics. It was tested for IDT predictions with modest success, as shown in Figure 2. The size of the model (141 species and 3609 reactions) is significantly larger than those models supplemented with additional data sets, and its generation required a much longer time. Therefore, an alternative model using libraries available in RMG, eventually including a library assembled for this study, combining the various modifications described below, was developed. The initial model employing multiple available libraries was denoted as "PN-ML" and utilizing tight tolerance parameters, consists of 100 species and 1333 reactions (about $1/6^{th}$ the number of species in the full NUIG mechanism).

Figure 2 compares experimental IDT data with predictions of three different models: (i) entirely estimate-based, PN-ES employing no built-in libraries; (ii) PN-CPL using only data from the NUIG model, CurranPentane library (CPL) as a source for both thermochemical properties and kinetics; and (iii) PN-ML model employing multiple libraries. The PN-ES model used only RMG estimation methods (GA and rate rules) to create a straightforward ("from scratch") model—without drawing on any prior modeling efforts or experimentally validated reaction kinetics (PN-ES). This estimate-based model generally reproduces the negative temperature coefficient (NTC) features, but the NTC region is significantly shifted to higher temperatures and shorter IDT, compared to the experimental data. The model generated using only data from the CPL for both reaction kinetics and thermochemistry (PN-CPL), performs somewhat better, in that the NTC is more nearly at the correct temperature range. Nonetheless, it produces notably worse predictions than the full NUIG model. The model generated using only CPL substantially overpredicts IDT across the NTC region. The results obtained using multiple libraries (PN-ML) were, for these conditions, quite similar to those using only CPL. The mechanism using multiple libraries was somewhat more compact (100 species, 1333 reactions for PN-ML vs 113 species, and 1454 reactions for PN-CPL) but was slightly further from predictions of the reference mechanism in the NTC region. Thus, drawing on available experimental and prior modeling studies is a rational approach to generating compact but broadly applicable mechanisms, but simply generating a mechanism using the most relevant built-in libraries remains inadequate. Additional analysis of the mechanism and rational modification of it are required, as described further below. Table S2 in the Supporting Information lists all the model variations discussed in this study.

One of the key model generation parameters, as noted above, is the "move to the core tolerance" threshold value for the selection of species based on their production rates. The lower the value of this tolerance, the greater the number of species that is included in the mechanism. To generate an adequate yet compact model, one must optimize this parameter. We studied the effect of tolerance on generation and performance and present IDT prediction results for the PN-ML models at tol = 0.01, 0.1, and 0.5 in Figure S8. Even though the PN-ML model generated with a tolerance of 0.5 shows remarkably good IDT prediction performance at 10 atm, closer inspection shows that lacks important species such as CO_2, atomic oxygen, two fuel (*n*-pentane) radicals, all isomers of pentene and C_5H_9 radicals. Thus, this agreement is fortuitous, and the model generated with tol = 0.5 was not considered further. The mechanism with tol = 0.1 includes all the important pathways, unlike the tol = 0.5 model, where C_5H_{10}/C_5H_9 chemistry is completely missing. We noted that the conjugated dimethylallyl radical C_5H_9 (434)—"$C_5H_9$2-4", the most stable isomer, was missing from the tol = 0.1 model prior to our modifications (discussed in detail in Section 3.2) that corrected the thermochemistry of the C_5 species. However, after the modifications, RMG included this important species in mechanisms generated with tol = 0.1. We encountered two main problems while generating a mechanism for tol = 0.01. First, mechanism generation never reached completion due to memory limitations. This is a common problem for RMG using a small tolerance for moving a species into the core mechanism. Working around this issue may be possible but was beyond the scope of this project. Second, it was computationally demanding and had already generated over 12 thousand reactions before running out of memory. Additionally, we hecked fluxes through key pathways for both tol = 0.1 and 0.01 models and found that the important pathways appeared for 0.1, as can be seen from Figures S5 and S11. The tol = 0.1 model correctly reproduced the roles of fuel radical generation and second oxygenation pathways at low temperatures in accord with general theory, as also follows from comparison of the sensitivity analyses and flux diagram pathway analysis. Thus, we selected the more compact model generated at tol = 0.1 to achieve a balance between prediction and compactness and focused on analyzing and refining this model. Table S4 compares the number of species and reactions for each of these cases, which shows that generation of the model with tol = 0.1 is an order of magnitude faster than that for tol = 0.01.

3.2. Collision Limit Violations and Improvement of Kinetic Parameters. Inspection of the RMG-generated models revealed several reactions violating collision rate limits. The extent to which they exceed the collision limit is characterized by a violation factor—the ratio of the rate coefficient to the collision limit rate at the relevant conditions.[47] Adjustment of rate parameters to avoid such violations of collision limits is a typical approach to improve kinetic models; for instance, the CPL library implemented in RMG includes 9 reactions "adjusted to correct TST and to achieve collision limits".[33]

Specifically, eight reactions in the PN-ML model have rate parameters that violate the collision limit. A common species present in most of the reactions is the acetyl $CH_3^{\bullet}CO$ radical. Because the violation factors identified by RMG are mostly small for these reactions—just slightly greater than unity, we did not modify these reactions. However, one reaction, the

https://doi.org/10.1021/acsomega.3c07079
ACS Omega 2023, 8, 49098−49114

Table 1. BDE and Formation Enthalpies (in kcal/mol) for Isomers of Pentene (C_5H_{10}) and Corresponding C_5H_9 Radicals Calculated at the G4MP2 Composite Level

species	notation	$\Delta_f H$ (298 K), (kcal/mol)	BDE, (kcal/mol)
1-pentene	PN-1*	−5.0 (−5.0 ± 2.0)[a]	
		−3.0[d]	
1-penten-1-yl	PN-1*1J	52.5	109.6
1-penten-2-yl	PN-1*2J	48.8	105.9
1-penten-3-yl (*1-ethylallyl*)	PN-1*3J	27.0	84.0
		28.4[b]; 26.83[c]	
1-penten-4-yl	PN-1*4J	39.5	96.6
		41.15[c]	
1-penten-5-yl	PN-1*5J	42.5	99.6
		41.4[b]; 43.59[c]	
2-pentene (*E*)	PN-2*	−7.1 (−7.7 ± 0.4)[a]	-
		−5.3[d]	
2-penten-1-yl (*1-ethylallyl*)	PN-2*1J	27.0	86.2
2-penten-2-yl (*1-ethyl-2-methyl-vinyl*)	PN-2*2J	47.1; 49.2[b]	106.3
2-penten-3-yl (*1-methyl-2-ethyl-vinyl*)	PN-2*3J	47.3	106.6
2-penten-4-yl (*1,3-dimethylallyl*)	PN-2*4J	24.5	83.7
2-penten-5-yl	PN-2*5J	40.1	99.3
		41.0[b]; 41.28[c]	

[a]Experimental data from NIST webbook https://webbook.nist.gov/chemistry. [b]RMG employed data from CPL-database. [c]Ref 28. [d]Calculated at CBS-QB3 level.

recombination of H atom with a linear isomer of C_5H_9 radical to form 2-pentene, appeared to be violating the collision limit by as much as 3 orders of magnitude—with violation factors equal to 2455 at 10 atm and 1739 at 1 atm. Note that C_5H_9 radical isomers participate in many reactions during pentane combustion and can potentially alter the ignition results. Therefore, this case was inspected in detail.

The violation ratio is typically due to inconsistency between the rate coefficient and the thermochemical data assigned to the species participating in the reaction. The C_5H_9 isomer of concern $CH_3C^{\bullet}{=}CHCH_2CH_3$ is one of only three isomers (out of nine) included by RMG in the model. It is denoted here as PN-2*2J, where numbers indicate carbon positions, * represents a double bond, and J a radical center (notation taken from ref 11). The other two isomers highlighted by RMG are PN-1*3J and PN-2*5J. To analyze why these three isomers were chosen specifically, we have analyzed bond dissociation enthalpies (BDE) for the formation of all possible C_5H_9 radicals derived from corresponding 1-, and 2-pentene isomers provided in Table 1 along with their formation enthalpies. The calculations were performed using the chemically accurate G4MP2 composite method and ARM-2 atomization approach.[45] In contrast to the popular CBS-QB3 method, which in this particular case substantially overestimates the formation enthalpies for molecular precursors, G4MP4 gives enthalpies of formation of the molecules, closely matching experimental results (Table 1).

Even though the dissociation enthalpy of the C(2)−H bond to form PN-2*2J is the highest among nine possible isomer formation channels (H-abstraction from 1- and 2-pentene), it is involved in several reactions in the RMG-generated model and can affect the overall reactivity. This isomer can be thought of as a double substituted vinyl radical: 1-ethyl-2-methyl vinyl $C_2H_5{-}CH{=}C^{\bullet}{-}CH_3$.

The other two RMG-generated isomers of C_5H_9 are PN-1*3J and PN-2*5J, while the overall most stable PN-2*4J isomer (*2,4-dimethylallyl*) derived from 2-pentene is missing. Notably, the model with CPL, when it is the only library, exclusively includes the last isomer PN-2*4J—thermodynamically the most favored one.

A nonphysical rate coefficient could be caused by mismatched assignments of the forward rate coefficient and species thermochemistry (more important at lower temperatures).[47] Therefore, we inspected the thermochemistry of C_5H_9 isomers (if the reason for violation was the molecular pentene 2-C_5H_{10}, then all isomers' rates would be affected). The first-principles-based enthalpy of formation for PN-2*2J isomer (ΔH_f^0 (298 K) = 47.1 kcal/mol) shows that RMG overestimated this value by 2.1 kcal/mol. The enthalpies of the other two isomers coming from the CPL library are in better agreement with G4MP2 data. The calculated enthalpy for PN-1*3J isomer perfectly matches, whereas that for the PN-1*5J isomer deviates in the reverse direction—somewhat underestimated (41.4 vs 42.5 at the G4MP2 level).

For comparison, the JetSurF2.0 high-temperature mechanism was also added as an additional data source, albeit with a lower priority than that of all other libraries, taking into account its high-temperature oriented character. It considers only 1-pentene precursor and correspondingly, includes its most easily formed isomers, viz., PN-1*3J (resonance stabilized *1-ethylallyl*), PN-1*4J, and PN-1*5J. Meanwhile, the CPL mechanism, involving both 1-, and 2-pentene species, additionally involves two other isomers of C_5H_9 derived from 2-pentene (PN-2*4J, and PN-2*5J).

The two remaining higher energy types of radicals not included in CPL are those derived from 1-PN: *1-propyl vinyl/2-propyl vinyl* radical, as well as *1-methyl-2-ethyl vinyl* radical derived from 2-pentane, being the structural isomer of the culprit PN-2*2J (*2-methyl-1-ethyl vinyl*) radical (Table 1). Thus, using the built-in rate rules and templates, RMG chooses three different isomers: PN-1*3J, PN-2*5J, and PN-2*2J. Whereas the first two could be considered reasonable selections based on their lower BDE and relative stability, the third one is clearly an anomaly, because it is one of the highest energy isomers and requires more than 106 kcal/mol energy to be directly generated (Table 1).

https://doi.org/10.1021/acsomega.3c07079
ACS Omega 2023, 8, 49098−49114

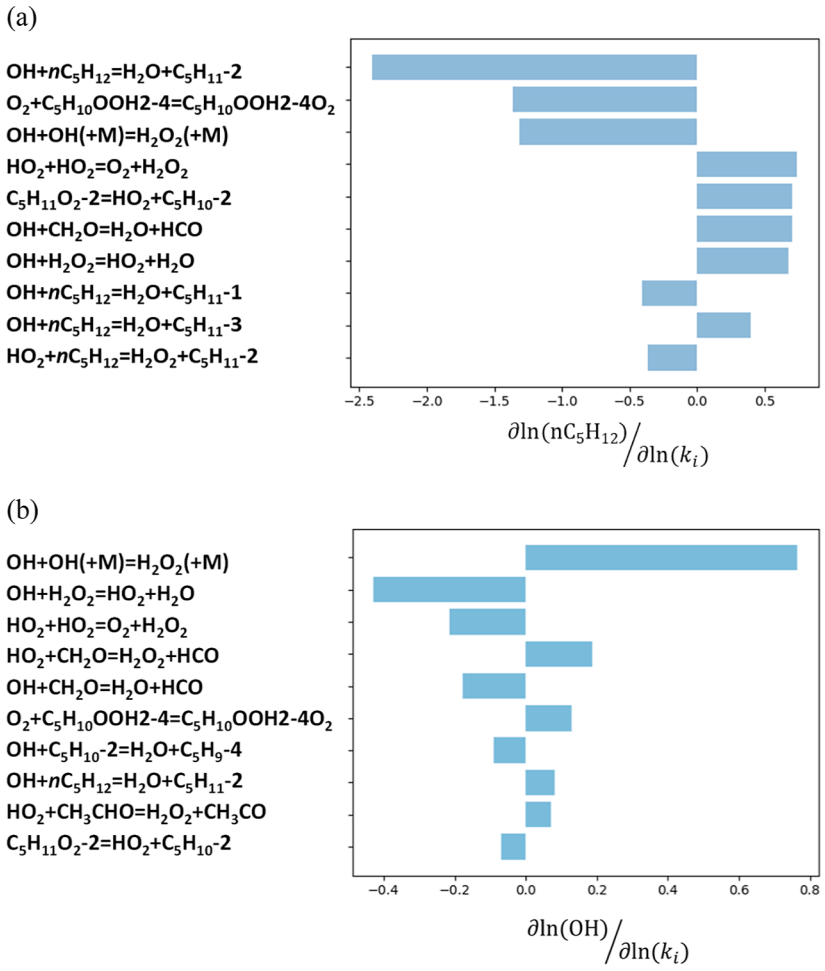

Figure 3. Sensitivity analysis, considering the maximum sensitivity of (a) pentane concentration and (b) OH concentration to reactions in the PN-ML mechanism at 750 K. The 10 reactions with highest absolute value of sensitivity coefficients are shown.

The problem can be related to errors associated with extrapolating a rate expression to low temperatures when the rate expression was obtained from high-temperature experiments.[47] The violation occurs only for low temperature conditions—both when *P*-dependence is included (with almost equal violation factors at 750 K for 1 and 10 atm), and when generation of *P*-dependent networks is excluded during mechanism generation (very high violation factor at 750 K and only 1.06 at 1350 K).

To examine the role of the violating reaction (recombination of H atom with a linear isomer of C_5H_9 radical to form 2-pentene, *vide supra*) in IDT simulations we have (a) replaced the violating rate coefficient with an alternative nonviolating value provided by RMG for analogous reactions of two other C_5H_9 isomer radicals, (b) excluded this reaction completely from the model evaluation, and (c) decreased the A-factor based on another value recently emerged from the RMG database. In all cases, we observed a negligible effect on IDT predictions (at P = 10 atm and ϕ = 2).

As noted above, the isomer of concern PN-2*2J (identical to PN-3*4J) can be represented as a substituted vinyl radical, $C_2H_5-CH{=}C^{\bullet}-CH_3$, *1-ethyl-2-methyl vinyl*. Because the H atom is the smallest possible radical to affect recombination dynamics, the violating reaction could also be mimicked by the even simpler recombination model reaction of H + C_2H_3 (vinyl radical) with reliable rate parameters taken, for instance, from the Klippenstein−Glarborg database as an upper bound, to test its possible effects. However, the employment of the newly assembled thermochemistry and kinetic RMG library also involving data from Table 1, guided RMG to generate an updated model excluding the collision-violating reaction described above. Moreover, the newly generated model also included the missing conjugated 1,3-*dimethylallyl* radical PN-2*4J - the most stable isomer among nine possible isomers of C_5H_9 radical with the highest probability to form. Consequently, the formation reaction of this radical from the 2-pentene precursor is also included in the list of most sensitive reactions at low temperatures, as described in the next section.

3.3. Model Refinements. *3.3.1. Refinements Based on Sensitivity Analysis.* To gain further insight and to improve predictions of the RMG-generated models, we conducted sensitivity analysis at constant temperature in RMG with a sensitivity threshold of 0.01. Reactions with the strongest influence on *n*-pentane concentration and formation of key pool radical OH were identified and analyzed, as shown in Figures 3 and 4 for T = 750 and 1150 K, respectively, where the normalized concentration sensitivities with respect to the reaction rate coefficients are provided.

As expected, the fuel (*n*-pentane) consumption is mostly governed by direct H-abstraction reactions along with some small species reactions with high fidelity rate parameters from the literature. The H-abstraction mostly occurs by OH radicals

https://doi.org/10.1021/acsomega.3c07079
ACS Omega 2023, 8, 49098−49114

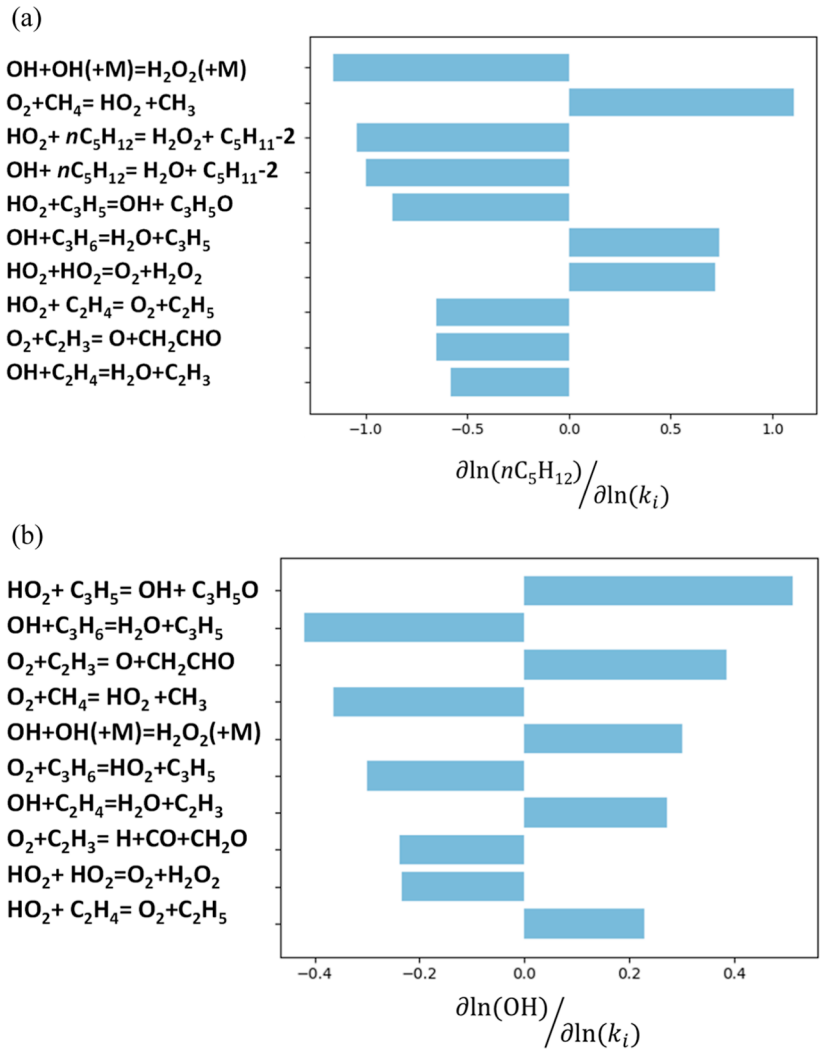

Figure 4. Sensitivity analysis, considering the maximum sensitivity of (a) pentane concentration and (b) OH concentration to reactions in the PN-ML mechanism at 1150 K. The 10 reactions with highest absolute value of sensitivity coefficients are shown.

to primarily form 2-pentyl radicals, in accord with theory.[11] In the same vein, the recombination of two OH and two HO_2 radicals also are among the most sensitive reactions. However, the rate coefficients for such small species reactions are also well-known from the literature and are included via employed databases (e.g., Klippenstein−Glarborg). Because there is relatively little uncertainty in the rate parameters of such reactions, we did not consider their modification here.

The low-temperature oxidation in the PN-ML mechanism, even where predictions are relatively poor, is mostly governed by peroxy chemistry, particularly the oxygenation of hydroperoxyalkyl (QOOH) radical, represented here as $C_5H_{10}OOH2{-}4$, and its HO_2-elimination to form 2-pentene. While the first reaction represents the main chain branching pathway for low temperatures, the second one leads to chain termination since HO_2 radical is relatively less reactive, in full accord with current understanding of the processes.[11,12,22,23,48,49] Therefore, the impact of the key low-T reactions identified by sensitivity analysis (750 K) involving peroxy chemistry, as listed in Figure 3, was explored further. The importance of peroxy chemistry is also shown in Figure S4.

Early investigations had assumed chain branching via reaction 1

$$RO_2 + RH \rightarrow ROOH \rightarrow RO + OH \quad (1)$$

to be the main chain-branching process,[23,48−50] however, the initial step in this sequence (the H-abstraction from a fuel molecule by an alkylperoxy radical), is typically too slow to explain experimental observations, as discussed by Taatjes and co-workers.[51,52] The more recent consensus has been that the "second O_2 addition"—the reaction of QOOH isomers with O_2, (reaction 3) is responsible for chain branching at low temperatures.

$$RO_2^{\bullet} \leftrightarrow {}^{\bullet}QOOH \quad (2)$$

$$O_2 + {}^{\bullet}QOOH \rightarrow {}^{\bullet}O_2QOOH(\rightarrow O{=}QOOH + OH) \quad (3)$$

$$O{=}QOOH \rightarrow OQ'O^{\bullet} + OH \quad (4)$$

The key experimental evidence provided by Taatjes and co-workers in 2009 using the cyclohexyl + O_2 reaction model,[51] and first-principles predictions available at the time on the corresponding low-lying pathways for pentane dual oxygenation,[53] confirmed this conjecture hypothesized half a century ago,[54−57] and employed in global kinetics modeling.[7,10,12,23,49,56,58] Figure 3 shows that this pathway, indeed, ranks high among the reactions in the sensitivity list for the

https://doi.org/10.1021/acsomega.3c07079
ACS Omega 2023, 8, 49098−49114

automatically generated *n*-pentane model at 750 K. The detailed analysis shows that both reactions 2 and 3 are influential, as expected from theory and simulations.[11,12,22−24,49,59] Use of rate parameters from the CPL database (when used as the only library) results in predicted IDTs that are notably longer than experimental measurements for *n*-pentane, at 10 atm and ϕ = 2 (PN-CPL, Figure 2).

Based on the discussion below (Section 3.4) on the effect of pressure dependent reactions on simulation results, high-pressure limit rate parameters for the second O_2-addition to *n*-hydroperoxypentyl (QOOH) radical obtained from a prior publication,[11] close to those alternatively provided by Truhlar and co-workers,[24] were tested and produced similarly good results. In particular, the rate parameters for the second O_2-addition, reaction 3 (written in Figure 3 as O_2 + $C_5H_{10}OOH2-4$ = $C_5H_{10}OOH2-4O_2$, where $C_5H_{10}OOH2-4$ and $C_5H_{10}OOH2-4O_2$ represent pentane-based hydroperoxyalkyl and hydroperoxyalkylperoxy radicals noted commonly as QOOH and O_2QOOH, respectively) were replaced with the high-*P* values presented in ref 11. The improved results for IDT in Section 3.4 agree with the conclusion by Bugler et al.[12,15,16] that *P*-dependent kinetics have little influence on these particular IDT predictions. With the updated rate coefficients for this reaction there is more flux from O_2QOOH radical to produce pentane keto-hydroperoxides (KHP, carbonyl-hydroperoxide) O=QOOH + OH, and subsequently, from dissociation of KHP, to yield a second OH and a carbonyl-oxy radical for chain branching (reaction 4).[11−16,21−26,28,49,59] Thus, we find that using the rate coefficients employed in CPL for the second O_2 addition, which are those of the first O_2-addition with the A-factors decreased by a factor of 2 and E_a reduced by 3 kcal/mol, results in IDT predictions that are much slower than experimental measurements for pentane. Whereas, replacing those with high-*P* rate parameters, included in a new library to employ in automatic model generation, yielded results in much better agreement with experimental observations (see Section 3.4). This is in accord with similar conclusions from a recent analysis by Xie et al. on oxidation of *n*-heptane.[60]

Further analysis of the sensitivity list at 750 K shows that the formation reaction of the most stable isomer of the pentenyl radical, the conjugated *dimethylallyl* radical PN-2*4J, derived from 2-pentene precursor (via also a sensitive reaction OH + C_5H_{10}-2 = H_2O + C_5H_9-4) is among most influential reactions involving OH radicals, which occurred after improvement of the thermochemistry (*vide supra*). Therefore, we also expect this pathway to alter the general model performance.

Turning to the sensitivity analysis at higher temperatures (1150 K), some other reactions were identified, mostly involving reactions of small species, as shown in Figure 4. As at 750 K, the main sensitive fuel consumption reactions correlate with those highlighted for OH-reactivity. The formation of HCO radical from O_2 + C_2H_3 reaction and its "prompt" dissociation as proposed by Klippenstein and co-workers,[55] is also among most influential reactions with the rate parameters provided at the highest theoretical level coming from Klippenstein−Glarborg library. Note that HCO radicals at lower temperatures are mostly formed from the OH + CH_2O reaction, as shown in Figure 3, and decompose only at higher temperatures. This reaction also comes from KG-library.

Another important reaction 5 is also highlighted in both sets of sensitivity diagrams (with respect to fuel molecules and OH-radicals) as an impactful reaction for combustion of hydrocarbons at mid and high temperatures.[61]

$$OH + C_2H_4 = H_2O + C_2H_3 \quad (5)$$

Historically, combustion models have assumed that the H_2O + vinyl radical products of reaction 5 are solely formed via the direct H-abstraction channel in a bimolecular collision of OH and ethylene. However, as shown in a series of studies,[62−64] these products can also arise from a roaming pathway to alter the overall reactivity. In a joint experimental/theoretical study, Kamarchik et al. demonstrated that the energized radical [$^{\bullet}CH_2CH_2OH$]*, formed by OH + C_2H_4 addition (or photolysis of haloethanols),[62] undergoes a dehydration reaction to form CH_2=$CH^{\bullet}$ + H_2O products passing through a flat region of the potential energy surface (explored by CBS-QB3 method) involving the transition complex [CH_2=$CH_2\cdots{}^{\bullet}OH$]. The phenomenon has been characterized as a roaming process.[64] In this case, the products form via frustrated dissociation of the activated CH_2CH_2OH radical back to OH + ethylene in which the C=O bond begins to stretch, but the leaving OH moiety abstracts an H atom to form H_2O + vinyl, thereby reducing the effective/overall kinetic barrier.[62] Further addition of O_2 to the generated vinyl radical is known to trigger multiple important chemically activated reactions.[61] Moreover, they can also involve roaming pathways. The increase in rate coefficient of the reaction of ethylene through reaction 5 due to more facilitated roaming has not previously been considered in the context of alkane combustion. However, the impact of roaming pathways has been generally studied by West and Goldsmith, using RMG, to predict possible impact of roaming pathways in a kinetic model.[65] They demonstrated that roaming can affect results primarily for the NTC region (as much as 40%).[65] Because reaction 5 appears in the fuel consumption sensitivity analysis at high *T*, we decided to test its effect overall. Keeping the overall rate of decomposition unchanged, the reaction was assumed by Goldsmith and West to branch into the regular bond fission and roaming channels.[65] Only the pre-exponential factor of the original bond fission reaction was modified, neglecting the temperature dependence of the roaming branching. About a 10% effect was found at low and high temperatures. Because the H-abstraction reaction of OH + C_2H_4 was not included, at least in a direct manner, in the analysis of the Goldsmith and West,[65] we decided to explore it further taking into account that due to roaming, the same product set (H_2O + C_2H_3) is formed via a more facilitated (on a flat PES region avoiding higher classical barrier) alternative pathway.[62]

$$OH + C_2H_4 \rightarrow [HOC_2H_4]^* \rightarrow H_2O + C_2H_3 \quad (6)$$

$$[HOC_2H_4]^* \rightarrow H_2O + C_2H_3 \text{ (via roaming)} \quad (7)$$

Thus, we increased the rate coefficient for reactions 6 and 7 provided in the RMG-PN mechanism by 40% to test its impact on the model global reactivity.

As noted above, the roaming can additionally alter the rate constants of some secondary reactions in the C_2H_3 + O_2 system, as discussed by Klippenstein.[61] Particularly, through the formation of long-range complex $CH_2CHO\cdots O$, which above 1700 K becomes predominantly a chain branching process. We have included this modification in our database for model generation because the formation of this set of products is already included in the list of sensitive reactions (Figure 4).

https://doi.org/10.1021/acsomega.3c07079
ACS Omega 2023, 8, 49098−49114

3.3.2. Other Refinements and Correction of Some Database-Induced Kinetic Parameters Employed by RMG. Another refinement was implemented to improve model reactivity including reaction 8 between the hydroperoxy radical and CO.

$$HO_2 + CO = OH + CO_2 \quad (8)$$

Fundamentally, the H_2/CO system plays an essential role in the hierarchical structure of combustion models of hydrocarbon fuels.[66−73] The most important reactions related to autoignition at mid-T and high-P are the chain-branching reaction H + O_2 = O + OH and the reactions involving H_2O_2 and HO_2,[23] yet reaction 8 has been considered to be the dominant reaction responsible for the mismatch of experimental and calculated ignition delay in the H_2/CO system at 950−1100 K, 15−50 bar, and ϕ = 0.36−1.6 conditions.[66,67,71] Therefore, we tested the effect of reaction 8 using alternative rate parameters to those employed by RMG. Reaction kinetics for this reaction have been extensively studied both experimentally[67,68,71−73] and theoretically.[66,69,70]

Using RMG with multiple libraries, the kinetic parameters for this reaction come from the single pathway analysis provided in the Klippenstein−Glarborg library in eq 9

$$k_8 = 1.60 \times 10^5 \times T^{2.18} e^{(17943\ \mathrm{cal}/RT)}\ \mathrm{cm}^3/\mathrm{mol}\cdot\mathrm{s} \quad (9)$$

The set of two rate constants provided in refs 66 and 70 represents two parallel pathways for reaction 8, denoted here as k_{8a} and k_{8b} and described by eqs 10 and 11, respectively, to separate chemical activation and bimolecular channels.

$$k_{8a} = 8.45 \times 10^8 \times T^{1.21} e^{(17267\ \mathrm{cal}/RT)}\ \mathrm{cm}^3/\mathrm{mol}\cdot\mathrm{s} \quad (10)$$

$$k_{8b} = 7.14\times10^7 \times T^{1.57} e^{(17267\ \mathrm{cal}/RT)}\ \mathrm{cm}^3/\mathrm{mol}\cdot\mathrm{s} \quad (11)$$

These rate constants are based on the potential energy surface explored by CBS-QB3 composite method combined with QRRK/master equation analysis.[66] Remarkably, these higher parallel-pathway kinetic parameters were shown to improve the simulation of IDTs for the H_2/CO system.[66,70] Therefore, to improve the pentane model performance, we updated the rate parameters for reaction 8 to include two channels with rate constants k_{8a} and k_{8b}. This modification, when used alone for particular high-pressure and fuel-rich conditions (P = 10 atm, ϕ = 2) had insignificant effect on IDT performance for pentane, which is consistent with literature on the combined effect of this reaction on model reactivity.[67,71] As noted by Mittal et al.,[67] the perturbation of reaction 8 alone does not dramatically alter the IDTs (for H_2/CO) as a hierarchical compound submodel, but in a proper combination it is effective. Therefore, we employed the rate constants described in eqs 10 and 11 and included them in the new library. Apparently, decreasing equivalence ratio (increasing O_2), promotes HO_2/H_2O_2 reactions, while reduction of O_2 can diminish HO_2/H_2O_2 chemistry.[67,71] Thus, HO_2 + CO becomes more important for fuel lean conditions.

During the model inspection, another issue was identified concerning the employed parameters of reaction 12, likely to be a transcription error.

$$HO_2 + C_2H_6 = H_2O_2 + C_2H_5 \quad (12)$$

The A-factor of 26 utilized in the rate coefficient $k_{12} = 2.60 \times 10^1 \times T^{3.37} e^{(15900\ \mathrm{cal}/RT)}$ cm^3/mol s should be increased by an order of magnitude (to 261 as reported in the original paper by Carstensen and co-workers[74]). Because the same authors subsequently revised this rate coefficient to even a higher value $k = 5.22 \times 10^3 \times T^{3.29} e^{(16000\ \mathrm{cal}/RT)}$ cm^3/mol s,[75] we chose to replace the erroneous rate coefficient by the more recent result.

The results show a modest effect in predictions at 10 atm and ϕ = 2, albeit in the right direction—improving the model performance at high temperatures.

We also carried out various tests in which we included data from the JetSurF2.0 database involving C_5−C_{12} oxidation chemistry, which, however, has been developed to reproduce primarily high-temperature processes.[76] As expected, in cases where RMG drew on properties from JetSurF2.0 for low-T chemistry rather than CPL, a lack of the detailed peroxy channels was observed. This led us to identify an incorrect value for the heat of formation of a key 2-pentyl radical, denoted as C_5H_{11}-2 in Figures 3 and 4, in the JetSurF2.0 database. We note that this value was correct in JetSurF1.0, but is dramatically higher in JetSurF2.0, effectively preventing formation of this radical.

3.4. Effect of the Modified Data Set on Model Performance. Incorporating the modifications described in Section 3.3 while generating a PN-ML mechanism resulted in PN-ML-m with 101 species and 1382 reactions. The 'm' in PN-ML-m mechanism denotes the modified and added database to our base mechanism (PN-ML). The IDT testing results against experimental data for the PN-ML-m model including multiple libraries (databases from most recent literature) but prioritizing the library of modified thermochemistry and rate parameters, along with PN-ML and PN-CPL for different fuel to oxidizer (equivalence) ratios (ϕ = 0.5, 1, and 2) and 10 atm conditions, are shown in Figure 5. This mechanism was generated while including P-dependent network generation using modified strong collision method.[33] A fuel rich system (ϕ = 2) is shown in Figure 5a, and NTC behavior is in good agreement with experiments and carefully tuned NUIG benchmark simulation results as opposed to the models PN-ML and PN-CPL. For ϕ = 1 the results reproduce NUIG RCM measurements even better than the original NUIG simulations (especially at lower temperatures). The same trend of improvements has been shown in Figure 5c for fuel lean conditions with better agreement to NUIG RCM results.

Furthermore, results for ϕ = 0.5, 1, and 2 at P = 10 atm show improvements after applying changes (PN-ML-m). The modifications described in Section 3.3 increase the reactivity in all cases at 10 atm, as shown in Figure 5. These changes confirmed the importance of changes for oxygen addition and chain branching reactions at lower temperatures that was thoroughly discussed in the previous section, along with other alternative databases. The applied modification effect in the reaction pathway at 723 K is shown in Figure S5. It shows the importance of the generation of ketohydroperoxide (KHP) intermediates at early ignition stages. More details on unimolecular decomposition of pentane-derived ketohydroperoxides will be reported separately.[77]

To further inspect the PN-ML-m mechanism at lower pressures, Figure 6 shows the IDT predictions utilized in databases at P = 1 atm. Figure S2 also shows the effect of the databases used for different mechanisms at lower pressures. The comparison for all equivalence ratios with available experimental data shows that the effect on IDT prediction is less significant at 1 atm compared to the effect at 10 atm. This is for the case in which pressure dependent reaction networks

https://doi.org/10.1021/acsomega.3c07079
ACS Omega 2023, 8, 49098−49114

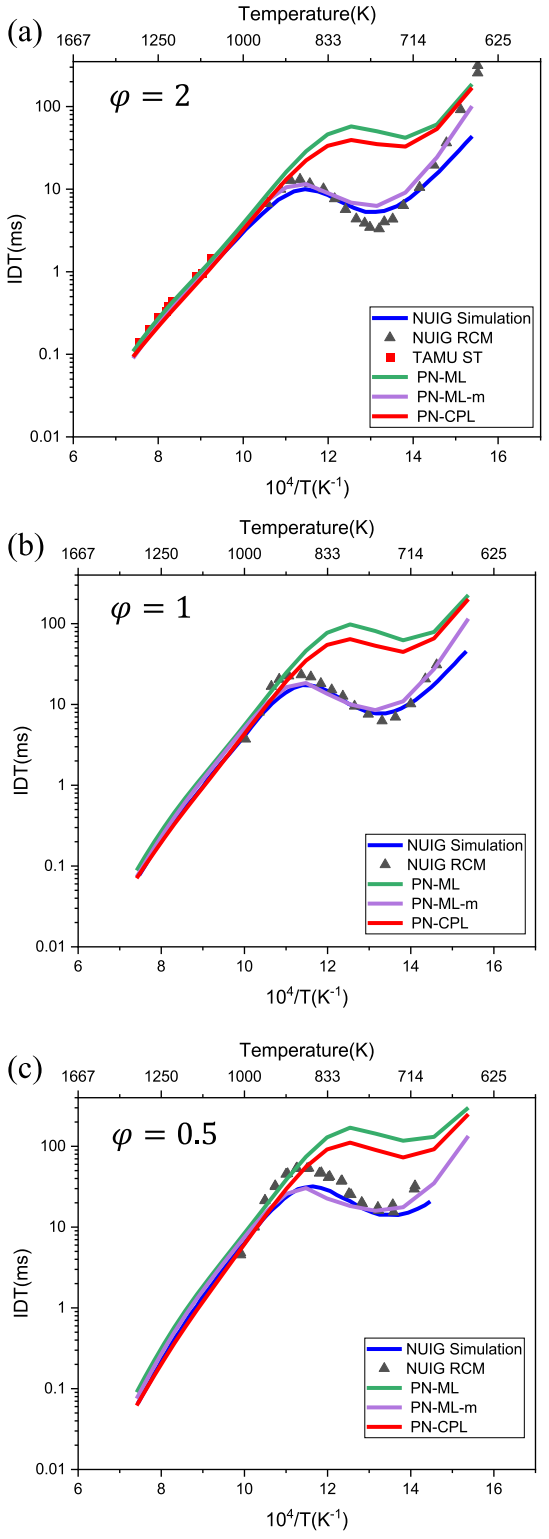

Figure 5. Effect of employed database on model performance at 10 atm: only the main library (PN-CPL), multiple libraries, as described in the text (PN-ML), and with the new library of modified parameters (PN-ML-m) were utilized. (a) ϕ = 2, (b) ϕ = 1, and (c) ϕ = 0.5. Symbols are experimental data; lines are model predictions.

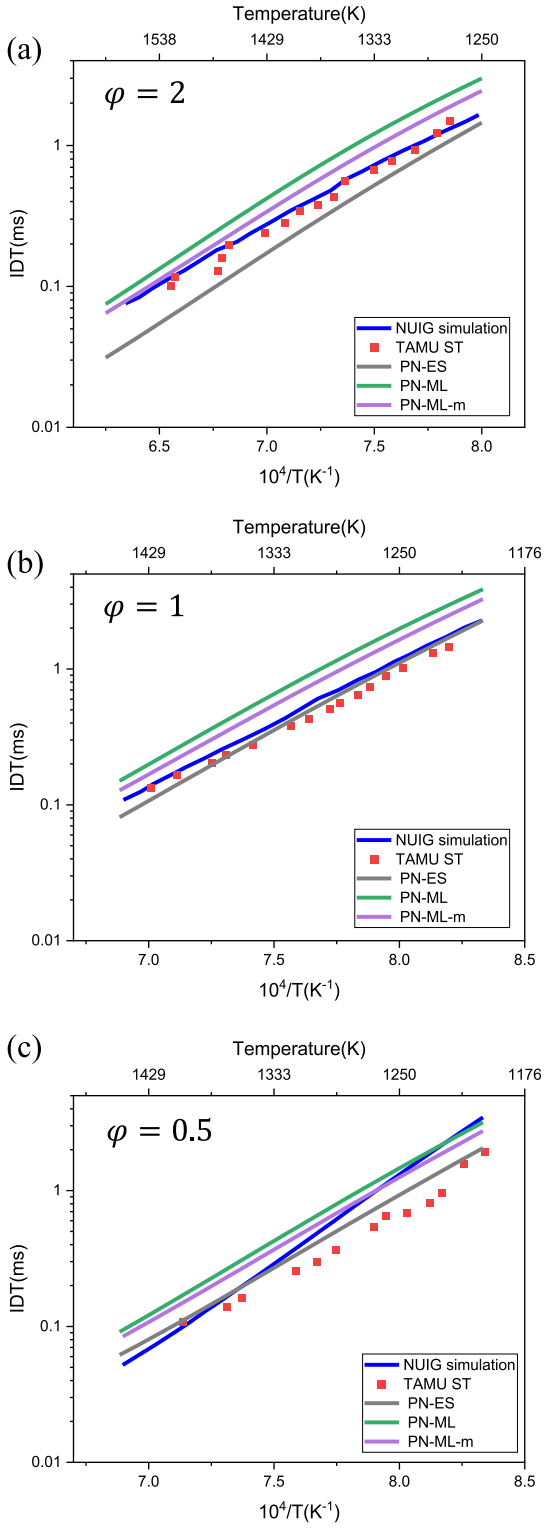

Figure 6. Effect of employed database at 1 atm: with no database used for thermochemistry or kinetics (PN-ES), multiple libraries (PN-ML), and modified data set (PN-ML-m). (a) ϕ = 2, (b) ϕ = 1, and (c) ϕ = 0.5. Symbols are experimental data; lines are model predictions.

are generated by RMG, along with pressure-dependent reactions taken from libraries. Nonetheless, the modifications made here bring the IDT predictions closer to the experiments and simulation from the literature. We note that this mechanism can be reduced further using methods such as directed relation graph with error propagation (DRGEP) or a global pathway selection (GPS).[34,35] While the rate-based algorithm of RMG is efficient in its inclusion of only the most relevant species in the generated mechanisms, it includes all reactions among the core species and thus may include many

https://doi.org/10.1021/acsomega.3c07079
ACS Omega 2023, 8, 49098−49114

unimportant reactions that could be systematically eliminated by mechanism reduction approaches.

3.5. Effect of *P*-Dependent Reactions of *n*-Pentane on Ignition Delay Simulations. *P*-dependent reactions constitute a significant part of the generated models, particularly involving reactions of small and medium-sized species and consuming a large fraction of the time required for mechanism generation. However, for large alkanes (paraffins), the effect of pressure on kinetics is expected to be more limited, especially for pressures greater than one atm. Direct description of high-pressure rate coefficients for large alkanes under most conditions relevant to combustion and ignition problems would largely simplify automated generation of kinetic models for larger systems. Neglect of pressure dependence is especially justified for larger alkanes because of their multitude of relaxation modes. This observation was also reported by Villano et al.,[78,79] as discussed above, when comparing reactivity of relatively small *n*-C_4H_{10}, medium size *n*-C_8H_{18}, and large *n*-$C_{12}H_{26}$ paraffins via analysis of the product distribution for oxidation with and without *P*-dependence. While no effect was found for the two larger molecules, a minor effect was seen for *n*-butane—the smallest alkane, which was studied under low-pressure conditions.

Therefore, we further explored the role of *P*-dependent reactions of *n*-pentane on IDT predictions using two types of automatically generated models—with and without *P*-dependence options. Note that the built-in libraries bring *P*-dependent reactions for smaller species into the newly generated models. For instance, the rate parameters for the small combination reaction H + C_2H_3 is taken by RMG from the Klippenstein–Glarborg library[41] (as one would expect). However, this is the case only when the *P*-dependent network generation was turned off in RMG. In contrast, during the *P*-dependent model generation, RMG generates its own pressure-dependent reaction network with estimated rate parameters. Thus, even for reactions of smaller species for which some rate parameters are available in libraries, RMG prioritizes the generation of the *P*-dependent network over the use of those data. Thus, the pressure dependent rate constants or the corresponding high-pressure values for *n*-pentane (and larger alkanes) can be achieved automatically by turning off and on the *P*-dependence in RMG mechanism development (while retaining the *P*-dependence for reactions of smaller species from previously defined libraries). Figure 7 compares IDTs for various cases in which different sets of database and estimation methods are used to test for fuel rich conditions. First, Figure 7a describes the case where no pressure dependent network generation was requested when there were no libraries used; "from scratch" models (PN-ES vs PN-ES-noPdep) are entirely based on RMG-estimations (rate rules and GA). Here, the generation of pressure-dependent reaction networks has an effect at the pressures and over the temperature range investigated due to the importance of *P*-dependent reactions of small species in PN-ES which are missing in the PN-ES-noPdep model. As seen, the IDT curve is shifted to mid temperatures and mostly undergoes changes at higher temperatures where small species reactions are responsible for ignition.

Figure 7b shows the same comparison but for the mechanisms using multiple recent databases (PN-ML-m vs PN-ML-m-noPdep) or only the CPL library (PN-CPL vs PN-CPL-noPdep) and how specifically requesting the generation of pressure dependent networks can alter the performance of the mechanism. The PN-ML-m-noPdep mechanism, which includes pressure-dependence of reactions from libraries but does not include any additional pressure-dependent networks generated during mechanism generation shows slightly decreased reactivity around first turnover (early stage of NTC region). However, the difference is more significant for PN-CPL-noPdep. This could be due to the contribution of other databases, libraries, with more pressure dependent reactions includedin the PN-ML-m mechanism (regardless of defining *P*-dependent network in RMG). Figure 8 also shows the performance for both stoichiometric and fuel lean conditions at high pressure (10 atm). As evident from both Figure 8a,b, the inclusion of pressure-dependent network generation improved the IDT predictions.

Decreased fuel reactivity (increased IDT) when excluding RMG-generated *P*-dependent reactions (by turning off *P*-

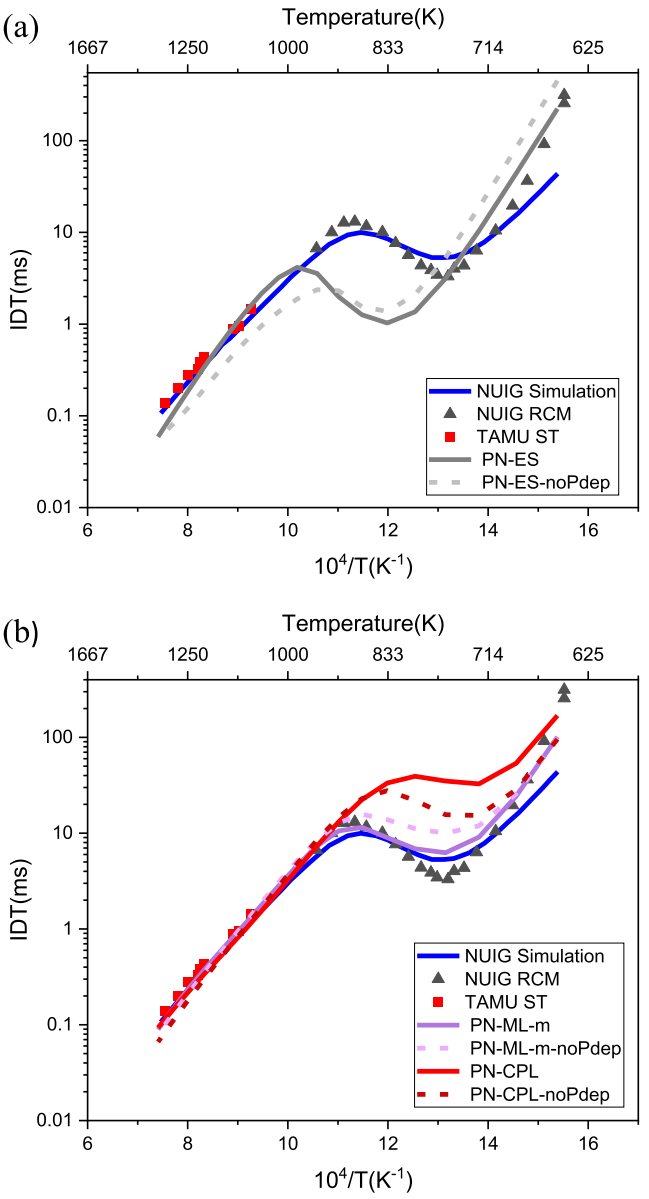

Figure 7. Modified (PN-ML-m) performance using multiple databases for equivalence ratio of 2 at 10 atm depending on the generation of *P*-dependent reaction networks. The mechanism without generation of *P*--dependent networks is labelled (noPdep) (a) models with no libraries, (b) models utilizing multiple databases and modified data set (PN-ML-m).

https://doi.org/10.1021/acsomega.3c07079
ACS Omega 2023, 8, 49098−49114

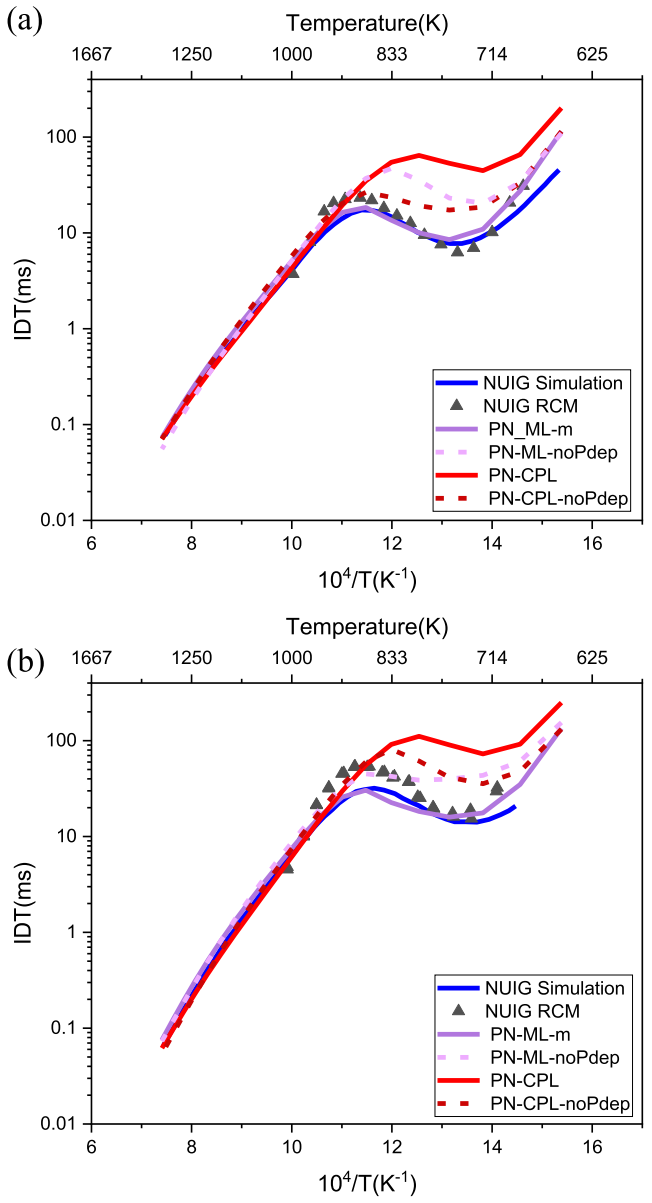

Figure 8. Effect of the inclusion of the *P*-dependent reaction network generation on IDT predictions at 10 atm. Exclusion of *P*-dependent network generation is indicated as (noPdep): multiple libraries and modified data set (PN-ML-m), only CPL (PN-CPL). (a) ϕ = 1, and (b) ϕ = 0.5. Symbols are experimental data; lines are model predictions.

dependent network generation), is seen in all cases illustrated in Figures 7 and 8 for ϕ = 2, 1, and 0.5. However, it is most prominent for stoichiometric and fuel lean conditions (Figure 8). The inspection of sensitivity lists discussed above shows that there are four sensitive reactions that are pressure dependent. These include two recombination reactions for OH and HO_2 radicals, whose rate parameters are taken from the employed libraries. They are not altered by including or excluding pressure-dependent network generation. Thus, two remaining unimolecular reactions are of greater interest: the second oxygenation reaction 3 and HO_2-elimination involving a 2-pentylperoxy radical ($C_5H_{11}O_2$-2) to form 2-pentene. Because the first reaction is a chain-branching reaction important to increase low temperature reactivity, its suppression is accountable for decreased reactivity and *vice versa*, the suppression of a termination reaction results in the increase of overall reactivity.

The above conclusions are consistent with results from the literature, such as those reported by Dean, Carstensen and co-workers,[78,79] along with the more recent studies on the *n*-propyl and *n*-butyl low temperature oxidation,[16,80,81] suggesting that pressure dependent effects may become greatly diminished at higher pressures (see also the discussion in ref 82).

Because the pressure dependence was found to have a noticeable effect on IDT simulations, we have developed both types of models in terms of *P*-dependence to be tested for more *P*-sensitive processes. Because pyrolysis/oxy-pyrolysis plays an important role in combustion of HRF and the major product ratios can vary significantly with pressure, the involvement of the *P*-dependent network may be more important to explore.

The effect of *P*-dependent reactions was tested for low pressure conditions in Figure 9 for all equivalence ratios at high temperatures, where experimental data are available. We used the same mechanisms used for the results in Figure 8. The results show an increase in reactivity, particularly for fuel rich and stoichiometric conditions. This aligns with an important conclusion from Villano et al. that the differences in the steady-state product distributions at high temperatures (1000 K) and low pressures (0.1 atm) occurred specifically for *n*-butane oxidation being the smallest considered alkane, as opposed to the much larger *n*-octane and *n*-dodecane oxidation.[78,79] Bugler et al. (2017)[16] have also studied this issue and successfully described the low temperature oxidation reactions of the pentane isomers using high-pressure limit rate coefficients.

Based upon these findings, we have also tested the role of the selected *P*-dependent reactions on automatically generated models' performance. The alternative high-pressure limit rate coefficients were tested for some of the most sensitive reactions identified by sensitivity analysis, as described in Section 3.3.1. As described above, all modified reactions and parameters were included in a separate library along with some other types of modifications to perform IDT simulations, and as can be seen from Figure 5 for models including *P*-dependent reactions and Figures 8 and 9 for those without pressure dependent network generation.

To summarize this section, we generated and tested two types of models in terms of *P*-dependence. The model with *P*-dependence is in better agreement with experiment (IDTs) for higher pressure (10 atm) conditions at lower temperatures. Further analysis provided below also shows that under typical engine conditions for combustion and ignition the high-pressure limit rate coefficients also could be used directly to automatically generate low-temperature oxidation chemistry without any further consideration of pressure effects for larger species.

3.6. Flame Speed Calculations. Premixed flame speed calculations were carried out using Cantera version (2.5.1). The laminar burning velocity, S_u (cm/s) of the PN-ML-m mechanism for atmospheric pressure at an initial temperature of 353 K was calculated and compared with three independent experimental reports[83−85] and one simulation using the NUIG full mechanism as shown in Figure 10a. The two experimental results are reported at 353 K and the Dirrenberger et al. experimental setup was at 358 K.

The comparison was generated for an equivalence ratio of 0.75 to 1.0 with an average error percentage of 8% in

https://doi.org/10.1021/acsomega.3c07079
ACS Omega 2023, 8, 49098−49114

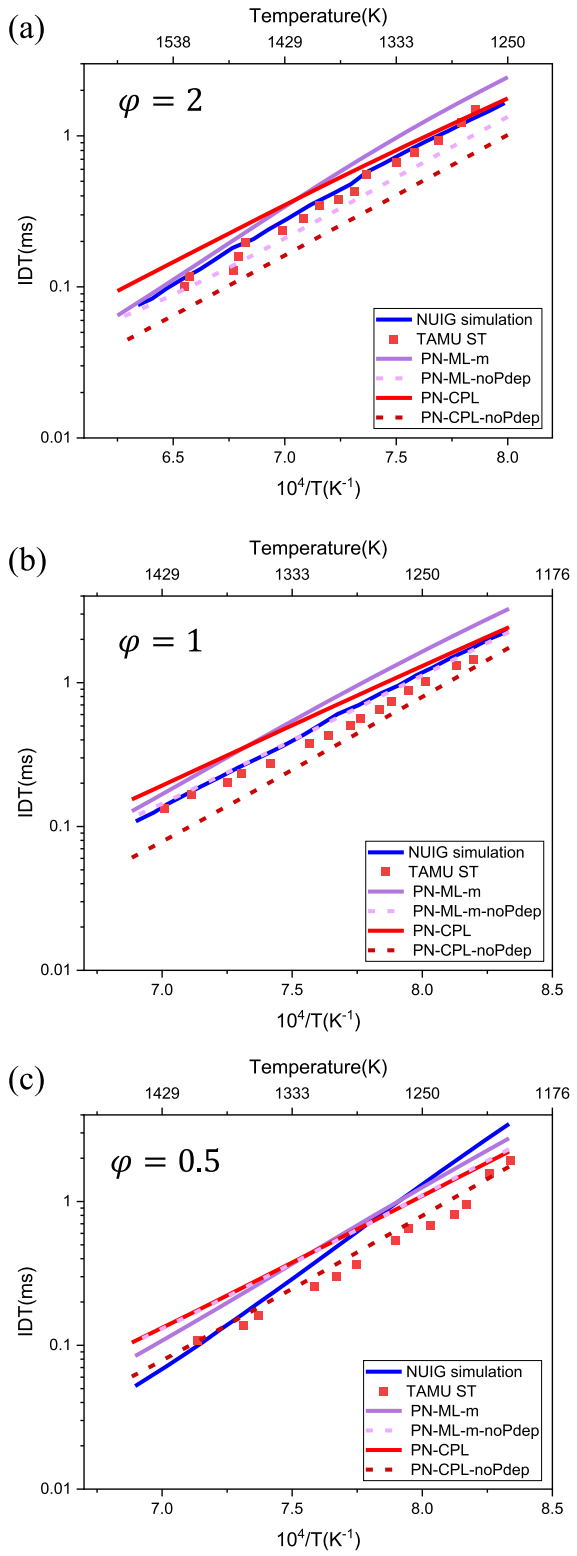

Figure 9. Effect of the inclusion of the *P*-dependent reaction network generation on the IDT predictions at 1 atm. Exclusion of *P*-dependent network generation is indicated as (noPdep): multiple libraries and modified data set (PN-ML-m), only CPL (PN-CPL). (a) $\phi = 2$, (b) $\phi = 1$, and (c) $\phi = 0.5$. Symbols are experimental data; lines are model predictions.

comparison with Kelley et al. at 353 K across the studied range. The comparison for other temperatures showed that the error percentage slightly increased with decreasing temperature from

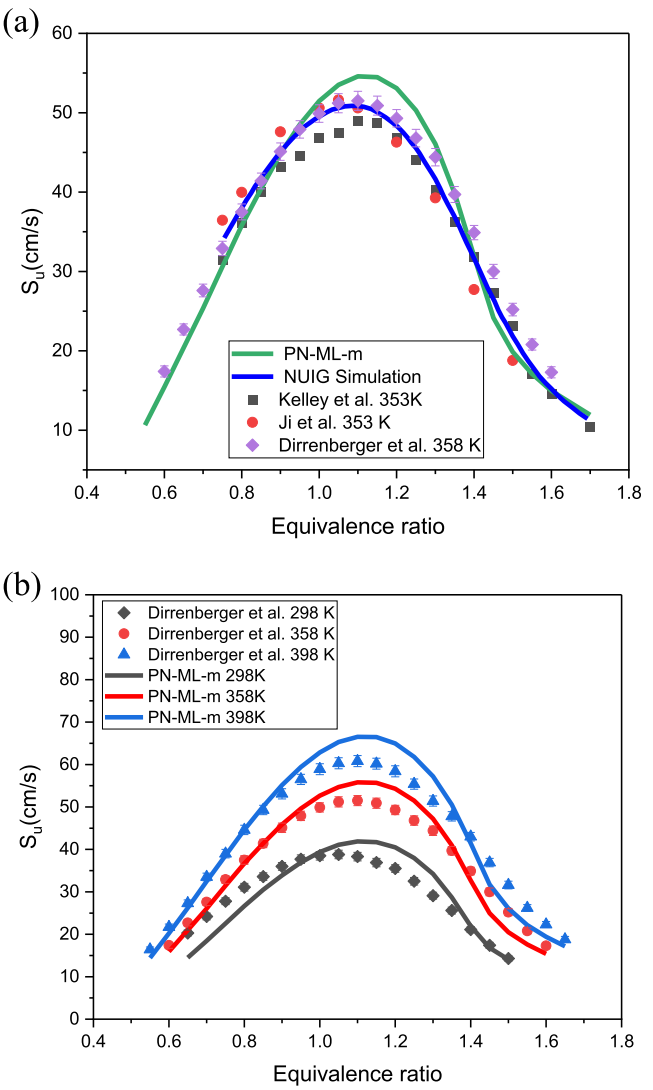

Figure 10. Flame speed comparison for PN-ML-m mechanism: (a) evaluated at 353 K, and (b) at temperatures of 298, 358, and 398 K. Symbols are experimental data; lines are model predictions.

an average of 7.8 to 11%. However, overall agreement with experiment was good, with differences between experiment and simulation comparable to differences between the independent experiments.

Kelley et al. have reported experimental data on the laminar flame speeds of *n*-pentane with air for elevated pressure (2, 5, and 10 atm) which we compared with predictions of the PN-ML-m mechanism, as shown in Figure 11. The error percentage decreases with decreasing pressure from 16% error to 5% from 10 to 2 atm, respectively.

The flame speed sensitivity analysis was also carried out for the pentane mechanism and showed the expected importance of OH, H, and HO_2 radicals (Figure S7).

4. CONCLUSIONS

Pentane is the smallest paraffin relevant to the combustion of large alkanes—paraffin wax, which is a promising HRF. We have developed an automatically generated compact mechanism for pentane combustion for a wide range of conditions, spanning high and low temperatures, three equivalence ratios (0.5, 1.0, 2.0), and pressures of 1 and 10 atm using an

https://doi.org/10.1021/acsomega.3c07079
ACS Omega 2023, 8, 49098−49114

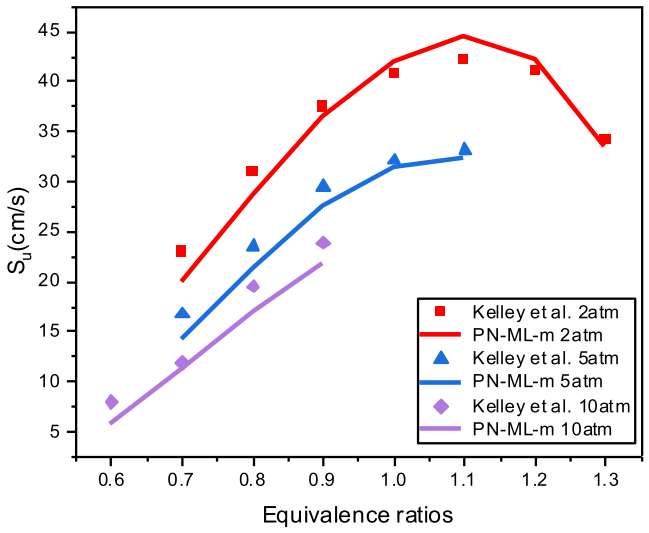

Figure 11. Flame speed comparison for the PN-ML-m mechanism. Symbols are experimental data; lines are model predictions.

automated software, RMG, and tested against global combustion characteristics of *n*-pentane. Different libraries of thermochemical and rate parameters and estimation methods were tested for use in model generation. The sensitivity and reaction path analyses confirmed the importance of dual oxygenation of fuel radicals for low-temperature chain branching and autoignition. We have further studied the important elementary reactions and provided improvements assembled in a separate library to complement the automatic generation of kinetic mechanisms for combustion of larger *n*-alkanes.

The final model denoted as PN-ML-m was validated against experimental and simulation IDT predictions for *n*-pentane across a range of temperatures (650 to 1350 K), pressures (1 to 10 atm), and equivalence ratios (0.5 to 2.0). It was also validated against flame speed measurements at pressures from 1 to 10 atm, 298 to 398 K, across fuel lean, stoichiometric, and fuel rich conditions. We note that we did not validate predictions of intermediate product concentrations at this stage but validated against global combustion characteristics of the fuel.

We also studied the effect of pressure dependent reaction networks on predicting global combustion characteristics of *n*-pentane. In accord with the literature, our results from IDT calculations and flame speed modeling show that model performance is mostly governed by the *P*-dependent networks of reactions among small species and is less sensitive to the *P*-dependent reaction networks generated by RMG for larger species, especially at higher pressures. We compared the effect of pressure dependent reactions and their importance for our considered range of conditions. Our results from IDT calculation and the flame speed show a good overall agreement for the final model incorporating several reasonable improvements, which were included in our created database.

Comparisons with the literature results also showed good performance for the final mechanism, denoted PN-ML-m, especially for the crucial NTC region, which is primarily based on the chemistry of peroxy and hydroperoxy radicals. This mechanism consisting of 1382 reactions and 101 species is substantially more compact than the manually developed benchmark full NUIG mechanism (~1/6th of the species) and may be particularly useful as a seed submechanism for automated generation of kinetic models for combustion of extra-large *n*-alkanes (paraffin-wax-surrogate-based HRFs) using RMG or similar approaches. Note, however, that the full NUIG mechanism treats all three pentane isomers as fuel, while the mechanism developed here considers only *n*-pentane.

■ ASSOCIATED CONTENT

Supporting Information

The Supporting Information is available free of charge at https://pubs.acs.org/doi/10.1021/acsomega.3c07079.

Difference between merged and ranged approaches; effect of modified database at 1 atm for all equivalence ratios; sensitivity analysis results with respect to concentration of HO_2 and H_2O_2 in the PN-ML mechanism at 750 and 1150 K, respectively; pathway analysis at 723 K, ϕ = 2 and 10 atm for before and after modifications; temperature sensitivity at 723 K before modifications (PN-ML); list of sensitive reactions with respect to the flame speed; mechanisms that were utilized in the paper; details on other RMG settings (different kind of tolerances was used for the model generation); effect of different tolerances on mechanism generation; number of species and reactions for different tolerances along with execution time for mechanism generation; comparison of all the changed rate parameters and rate constants at two temperatures; comparison of the rate constants for eqs 1, 9, 10, and 11 respectively; and pathway analysis before modifications (PN-ML) for tol = 0.01. All these mechanisms are publicly available on GitHub at https://github.com/UBCHREST/reactionMechanisms (PDF)

■ AUTHOR INFORMATION

Corresponding Author

Mark Swihart − *Department of Chemical and Biological Engineering, University at Buffalo, The State University of New York, Buffalo, New York 14260, United States;* orcid.org/0000-0002-9652-687X; Email: swihart@buffalo.edu

Authors

Venus Amiri − *Department of Chemical and Biological Engineering, University at Buffalo, The State University of New York, Buffalo, New York 14260, United States*

Rubik Asatryan − *Department of Chemical and Biological Engineering, University at Buffalo, The State University of New York, Buffalo, New York 14260, United States;* orcid.org/0000-0003-1200-2727

Complete contact information is available at: https://pubs.acs.org/10.1021/acsomega.3c07079

Author Contributions

The manuscript was written through contributions of all authors. All authors have given approval to the final version of the manuscript.

Notes

The authors declare no competing financial interest.

■ ACKNOWLEDGMENTS

This research is funded by the United States Department of Energy's (DoE) National Nuclear Security Administration

(NNSA) under the Predictive Science Academic Alliance Program III (PSAAP III) at the University at Buffalo, under contract number DE-NA0003961. Computing time was provided by the UB Center for Computational Research.

REFERENCES

(1) Jens, E. T.; Cantwell, B. J.; Hubbard, G. S. Hybrid rocket propulsion systems for outer planet exploration missions. *Acta Astronaut.* **2016**, *128*, 119−130.
(2) Petrarolo, A.; Kobald, M.; Schlechtriem, S. Optical analysis of the liquid layer combustion of paraffin-based hybrid rocket fuels. *Acta Astronaut.* **2019**, *158*, 313−322.
(3) Leccese, G.; Cavallini, E.; Pizzarelli, M. State of Art and Current Challenges of the Paraffin-Based Hybrid Rocket Technology. *AIAA Propulsion and Energy 2019 Forum*; American Institute of Aeronautics and Astronautics, 2019.
(4) Migliorino, M. T.; Bianchi, D.; Nasuti, F. Numerical Analysis of Paraffin-Wax/Oxygen Hybrid Rocket Engines. *J. Propul. Power* **2020**, *36* (6), 806−819.
(5) Carrick, P. G. Theoretical performance of high energy density cryogenic solid rocket propellants. *31st Joint Propulsion Conference and Exhibit*: San Diego, CA, 1995.
(6) Carrick, P. G.; Larson, W. C. Lab scale test and evaluation of cryogenic solid hybrid rocket fuels. *31st Joint Propulsion Conference and Exhibit*: San Diego, CA, 1995.
(7) Westbrook, C. K.; Pitz, W. J.; Thornton, M. M.; Malte, P. C. A kinetic modeling study of *n*-pentane oxidation in a well-stirred reactor. *Combust. Flame* **1988**, *72* (1), 45−62.
(8) Minetti, R.; Roubaud, A.; Therssen, E.; Ribaucour, M.; Sochet, L. R. The chemistry of pre-ignition of *n*-pentane and 1-pentene. *Combust. Flame* **1999**, *118* (1−2), 213−220.
(9) Zhukov, V. P.; Sechenov, V. A.; Starikovskii, A. Y. Self-ignition of a lean mixture of *n*-pentane and air over a wide range of pressures. *Combust. Flame* **2005**, *140* (3), 196−203.
(10) Ribaucour, M.; Minetti, R.; Sochet, L. R.; Curran, H. J.; Pitz, W. J.; Westbrook, C. K. Ignition of isomers of pentane: An experimental and kinetic modeling study. *Proc. Combust. Inst.* **2000**, *28* (2), 1671−1678.
(11) Asatryan, R.; Bozzelli, J. W. Chain Branching and Termination in the Low-Temperature Combustion of n-Alkanes: 2-Pentyl Radical + O_2, Isomerization and Association of the Second O_2. *J. Phys. Chem. A* **2010**, *114* (29), 7693−7708.
(12) Bugler, J.; Somers, K. P.; Silke, E. J.; Curran, H. J. Revisiting the Kinetics and Thermodynamics of the Low-Temperature Oxidation Pathways of Alkanes: A Case Study of the Three Pentane Isomers. *J. Phys. Chem. A* **2015**, *119* (28), 7510−7527.
(13) Rodriguez, A.; Herbinet, O.; Wang, Z.; Qi, F.; Fittschen, C.; Westmoreland, P. R.; Battin-Leclerc, F. Measuring hydroperoxide chain-branching agents during *n*-pentane low-temperature oxidation. *Proc. Combust. Inst.* **2017**, *36* (1), 333−342.
(14) Tran, L.-S.; Li, Y.; Zeng, M.; Pieper, J.; Qi, F.; Battin-Leclerc, F.; Kohse-Höinghaus, K.; Herbinet, O. Elevated pressure low-temperature oxidation of linear five-heavy-atom fuels: diethyl ether, *n*-pentane, and their mixture. *Z. Phys. Chem.* **2020**, *234* (7−9), 1269−1293.
(15) Bugler, J.; Marks, B.; Mathieu, O.; Archuleta, R.; Camou, A.; Grégoire, C.; Heufer, K. A.; Petersen, E. L.; Curran, H. J. An ignition delay time and chemical kinetic modeling study of the pentane isomers. *Combust. Flame* **2016**, *163*, 138−156.
(16) Bugler, J.; Rodriguez, A.; Herbinet, O.; Battin-Leclerc, F.; Togbé, C.; Dayma, G.; Dagaut, P.; Curran, H. J. An experimental and modelling study of *n*-pentane oxidation in two jet-stirred reactors: The importance of pressure-dependent kinetics and new reaction pathways. *Proc. Combust. Inst.* **2017**, *36* (1), 441−448.
(17) Bu, L.; Ciesielski, P. N.; Robichaud, D. J.; Kim, S.; McCormick, R. L.; Foust, T. D.; Nimlos, M. R. Understanding Trends in Autoignition of Biofuels: Homologous Series of Oxygenated C_5 Molecules. *J. Phys. Chem. A* **2017**, *121* (29), 5475−5486.
(18) Cheng, Y.; Hu, E.; Lu, X.; Li, X.; Gong, J.; Li, Q.; Huang, Z. Experimental and kinetic study of pentene isomers and *n*-pentane in laminar flames. *Proc. Combust. Inst.* **2017**, *36* (1), 1279−1286.
(19) Catoire, L.; Swihart, M. T.; Gail, S.; Dagaut, P. Anharmonic thermochemistry of cyclopentadiene derivatives. *Int. J. Chem. Kinet.* **2003**, *35* (9), 453−463.
(20) Sharma, S.; Raman, S.; Green, W. H. Intramolecular Hydrogen Migration in Alkylperoxy and Hydroperoxyalkylperoxy Radicals: Accurate Treatment of Hindered Rotors. *J. Phys. Chem. A* **2010**, *114* (18), 5689−5701.
(21) Zhu, L.; Bozzelli, J. W.; Kardos, L. M. Thermochemical Properties, $\Delta_f H°(298)$, $S°(298)$, and $C_p°(T)$, for *n*-Butyl and *n*-Pentyl Hydroperoxides and the Alkyl and Peroxy Radicals, Transition States, and Kinetics for Intramolecular Hydrogen Shift Reactions of the Peroxy Radicals. *J. Phys. Chem. A* **2007**, *111* (28), 6361−6377.
(22) Klippenstein, S. J. From theoretical reaction dynamics to chemical modeling of combustion. *Proc. Combust. Inst.* **2017**, *36* (1), 77−111.
(23) Zádor, J.; Taatjes, C. A.; Fernandes, R. X. Kinetics of elementary reactions in low-temperature autoignition chemistry. *Prog. Energy Combust. Sci.* **2011**, *37* (4), 371−421.
(24) Xing, L.; Bao, J. L.; Wang, Z.; Wang, X.; Truhlar, D. G. Hydrogen shift isomerizations in the kinetics of the second oxidation mechanism of alkane combustion. Reactions of the hydroperoxypentylperoxy OOQOOH radical. *Combust. Flame* **2018**, *197*, 88−101.
(25) Wang, Z.; Chen, B.; Moshammer, K.; Popolan-Vaida, D. M.; Sioud, S.; Shankar, V. S. B.; Vuilleumier, D.; Tao, T.; Ruwe, L.; Bräuer, E.; et al. *n*-Heptane cool flame chemistry: Unraveling intermediate species measured in a stirred reactor and motored engine. *Combust. Flame* **2018**, *187*, 199−216.
(26) Sahetchian, K. A.; Rigny, R.; Circan, S. Identification of the hydroperoxide formed by isomerization reactions during the oxidation of *n*-heptane in a reactor and CFR engine. *Combust. Flame* **1991**, *85* (3−4), 511−514.
(27) Ranzi, E.; Cavallotti, C.; Cuoci, A.; Frassoldati, A.; Pelucchi, M.; Faravelli, T. New reaction classes in the kinetic modeling of low temperature oxidation of *n*-alkanes. *Combust. Flame* **2015**, *162* (5), 1679−1691.
(28) Mehl, M.; Pitz, W. J.; Westbrook, C. K.; Curran, H. J. Kinetic modeling of gasoline surrogate components and mixtures under engine conditions. *Proc. Combust. Inst.* **2011**, *33* (1), 193−200.
(29) Blurock, E.; Battin-Leclerc, F.; Faravelli, T.; Green, W. H. Automatic Generation of Detailed Mechanisms. *Cleaner Combustion: Developing Detailed Chemical Kinetic Models*; Battin-Leclerc, F., Simmie, J. M., Blurock, E., Eds.; Springer London, 2013; pp 59−92.
(30) Van de Vijver, R.; Vandewiele, N. M.; Bhoorasingh, P. L.; Slakman, B. L.; Seyedzadeh Khanshan, F.; Carstensen, H.-H.; Reyniers, M.-F.; Marin, G. B.; West, R. H.; Van Geem, K. M. Automatic Mechanism and Kinetic Model Generation for Gas- and Solution-Phase Processes: A Perspective on Best Practices, Recent Advances, and Future Challenges. *Int. J. Chem. Kinet.* **2015**, *47* (4), 199−231.
(31) Broadbelt, L. J.; Pfaendtner, J. Lexicography of kinetic modeling of complex reaction networks. *AIChE J.* **2005**, *51* (8), 2112−2121.
(32) Battin-Leclerc, F.; Blurock, E.; Bounaceur, R.; Fournet, R.; Glaude, P.-A.; Herbinet, O.; Sirjean, B.; Warth, V. Towards cleaner combustion engines through groundbreaking detailed chemical kinetic models. *Chem. Soc. Rev.* **2011**, *40* (9), 4762−4782.
(33) Gao, C. W.; Allen, J. W.; Green, W. H.; West, R. H. Reaction Mechanism Generator: Automatic construction of chemical kinetic mechanisms. *Comput. Phys. Commun.* **2016**, *203*, 212−225.
(34) Niemeyer, K. E.; Sung, C.-J.; Raju, M. P. Skeletal mechanism generation for surrogate fuels using directed relation graph with error propagation and sensitivity analysis. *Combust. Flame* **2010**, *157* (9), 1760−1770.
(35) Gao, X.; Yang, S.; Sun, W. A global pathway selection algorithm for the reduction of detailed chemical kinetic mechanisms. *Combust. Flame* **2016**, *167*, 238−247.

https://doi.org/10.1021/acsomega.3c07079
ACS Omega 2023, 8, 49098−49114

(36) Zhao, H.; Dana, A. G.; Zhang, Z.; Green, W. H.; Ju, Y. Experimental and modeling study of the mutual oxidation of *n*-pentane and nitrogen dioxide at low and high temperatures in a jet stirred reactor. *Energy* **2018**, *165*, 727−738.
(37) Pio, G.; Dong, X.; Salzano, E. H.; Green, W. Automatically generated model for light alkene combustion. *Combust. Flame* **2022**, *241*, 112080.
(38) Kreitz, B.; Lott, P.; Bae, J.; Blöndal, K.; Angeli, S.; Ulissi, Z. W.; Studt, F.; Goldsmith, C. F.; Deutschmann, O. Detailed Microkinetics for the Oxidation of Exhaust Gas Emissions through Automated Mechanism Generation. *ACS Catal.* **2022**, *12* (18), 11137−11151.
(39) *CHEMKIN-PRO 15112 Reaction Design*: San Diego, 2011.
(40) Burke, M. P.; Chaos, M.; Ju, Y.; Dryer, F. L.; Klippenstein, S. J. Comprehensive H_2/O_2 kinetic model for high-pressure combustion. *Int. J. Chem. Kinet.* **2012**, *44* (7), 444−474.
(41) Hashemi, H.; Jacobsen, J. G.; Rasmussen, C. T.; Christensen, J. M.; Glarborg, P.; Gersen, S.; van Essen, M.; Levinsky, H. B.; Klippenstein, S. J. High-pressure oxidation of ethane. *Combust. Flame* **2017**, *182*, 150−166.
(42) Goldsmith, C. F.; Magoon, G. R.; Green, W. H. Database of Small Molecule Thermochemistry for Combustion. *J. Phys. Chem. A* **2012**, *116* (36), 9033−9057.
(43) Ritter, E. R.; Bozzelli, J. W. THERM: Thermodynamic property estimation for gas phase radicals and molecules. *Int. J. Chem. Kinet.* **1991**, *23* (9), 767−778.
(44) Frisch, M. J.; Trucks, G. W.; Schlegel, H. B.; Scuseria, G. E.; Robb, M. A.; Cheeseman, J. R.; Scalmani, G.; Barone, V.; Petersson, G. A.; Nakatsuji, H. et al. *Gaussian 16*, Revision A.03; Gaussian, Inc.: Wallingford, CT, 2016.
(45) Asatryan, R.; Bozzelli, J. W.; Simmie, J. M. Thermochemistry of Methyl and Ethyl Nitro, RNO_2, and Nitrite, RONO, Organic Compounds. *J. Phys. Chem. A* **2008**, *112* (14), 3172−3185.
(46) Liu, M.; Grinberg Dana, A.; Johnson, M. S.; Goldman, M. J.; Jocher, A.; Payne, A. M.; Grambow, C. A.; Han, K.; Yee, N. W.; Mazeau, E. J.; et al. Reaction Mechanism Generator v3.0: Advances in Automatic Mechanism Generation. *J. Chem. Inf. Model.* **2021**, *61* (6), 2686−2696.
(47) Chen, D.; Wang, K.; Wang, H. Violation of collision limit in recently published reaction models. *Combust. Flame* **2017**, *186*, 208−210.
(48) Westbrook, C. K.; Mehl, M.; Pitz, W. J.; Kukkadapu, G.; Wagnon, S.; Zhang, K. Multi-fuel surrogate chemical kinetic mechanisms for real world applications. *Phys. Chem. Chem. Phys.* **2018**, *20* (16), 10588−10606.
(49) Wang, Z.; Herbinet, O.; Hansen, N.; Battin-Leclerc, F. Exploring hydroperoxides in combustion: History, recent advances and perspectives. *Prog. Energy Combust. Sci.* **2019**, *73*, 132−181.
(50) Walker, R. W.; Morley, C. Chapter 1 Basic chemistry of combustion. *Comprehensive Chemical Kinetics*; Pilling, M. J., Ed.; Elsevier, 1997; Vol. *35*, pp 1−124.
(51) Fernandes, R. X.; Zádor, J.; Jusinski, L. E.; Miller, J. A.; Taatjes, C. A. Formally direct pathways and low-temperature chain branching in hydrocarbon autoignition: the cyclohexyl + O_2 reaction at high pressure. *Phys. Chem. Chem. Phys.* **2009**, *11* (9), 1320−1327.
(52) Savee, J. D.; Papajak, E.; Rotavera, B.; Huang, H.; Eskola, A. J.; Welz, O.; Sheps, L.; Taatjes, C. A.; Zádor, J.; Osborn, D. L. Direct observation and kinetics of a hydroperoxyalkyl radical (QOOH). *Science* **2015**, *347* (6222), 643−646.
(53) Asatryan, R.; Bozzelli, J. Chain branching and termination paths in oxidation of *n*-alkanes: Comprehensive Complete Basis Set-QB3 study on the association of *n*-pentyl radical with O_2, isomerization and addition of second oxygen molecule. *Technical Meeting of the Eastern States Section of the Combustion Institute*: Charlottesville, VA, 2007.32nd International Symposium on Combustion: Montreal, Canada, 2008
(54) Fish, A. Chain Propagation in the Oxidation of Alkyl Radicals. *Oxidation of Organic Compounds*; *Advances in Chemistry*; American Chemical Society, 1968; Vol. *76*, pp 69−85.
(55) Labbe, N. J.; Sivaramakrishnan, R.; Goldsmith, C. F.; Georgievskii, Y.; Miller, J. A.; Klippenstein, S. J. Weakly Bound Free Radicals in Combustion: "Prompt" Dissociation of Formyl Radicals and Its Effect on Laminar Flame Speeds. *J. Phys. Chem. Lett.* **2016**, *7* (1), 85−89.
(56) Benson, S. W. The kinetics and thermochemistry of chemical oxidation with application to combustion and flames. *Prog. Energy Combust. Sci.* **1981**, *7* (2), 125−134.
(57) Cox, R. A.; Cole, J. A. Chemical aspects of the autoignition of hydrocarbon air mixtures. *Combust. Flame* **1985**, *60* (2), 109−123.
(58) Westbrook, C. K. Chemical kinetics of hydrocarbon ignition in practical combustion systems. *Proc. Combust. Inst.* **2000**, *28* (2), 1563−1577.
(59) Sahetchian, K.; Champoussin, J. C.; Brun, M.; Levy, N.; Blin-Simiand, N.; Aligrot, C.; Jorand, F.; Socoliuc, M.; Heiss, A.; Guerassi, N. Experimental study and modeling of dodecane ignition in a diesel engine. *Combust. Flame* **1995**, *103* (3), 207−220.
(60) Xie, C.; Lailliau, M.; Issayev, G.; Xu, Q.; Chen, W.; Dagaut, P.; Farooq, A.; Sarathy, S. M.; Wei, L.; Wang, Z. Revisiting low temperature oxidation chemistry of *n*-heptane. *Combust. Flame* **2022**, *242*, 112177.
(61) Goldsmith, C. F.; Harding, L. B.; Georgievskii, Y.; Miller, J. A.; Klippenstein, S. J. Temperature and Pressure-Dependent Rate Coefficients for the Reaction of Vinyl Radical with Molecular Oxygen. *J. Phys. Chem. A* **2015**, *119* (28), 7766−7779.
(62) Kamarchik, E.; Koziol, L.; Reisler, H.; Bowman, J. M.; Krylov, A. I. Roaming Pathway Leading to Unexpected Water + Vinyl Products in C_2H_4OH Dissociation. *J. Phys. Chem. Lett.* **2010**, *1* (20), 3058−3065.
(63) Ratliff, B. J.; Alligood, B. W.; Butler, L. J.; Lee, S.-H.; Lin, J. J.-M. Product Branching from the CH_2CH_2OH Radical Intermediate of the OH + Ethene Reaction. *J. Phys. Chem. A* **2011**, *115* (33), 9097−9110.
(64) Suits, A. G. Roaming Reactions and Dynamics in the van der Waals Region. *Annu. Rev. Phys. Chem.* **2020**, *71*, 77−100.
(65) West, R. H.; Goldsmith, C. F. The impact of roaming radicals on the combustion properties of transportation fuels. *Combust. Flame* **2018**, *194*, 387−395.
(66) Bozzelli, J. W.; Asatryan, R.; Montgomery, C. J.; Sheng, C. Y. Pressure dependent mechanism for H/O/C(1) chemistry. *5th US Combustion Meeting*: San Diego, 2007.
(67) Mittal, G.; Sung, C.-J.; Yetter, R. A. Autoignition of H_2/CO at elevated pressures in a rapid compression machine. *Int. J. Chem. Kinet.* **2006**, *38* (8), 516−529. (acccessed 2022/10/10)
(68) Arustamyan, A. M.; Shakhnazaryan, I. K.; Philipossyan, A. G.; Nalbandyan, A. B. The kinetics and the mechanism of the oxidation of carbon monoxide in the presence of hydrogen. *Int. J. Chem. Kinet.* **1980**, *12* (1), 55−75.
(69) You, X.; Wang, H.; Goos, E.; Sung, C.-J.; Klippenstein, S. J. Reaction Kinetics of CO + HO_2 → Products: Ab Initio Transition State Theory Study with Master Equation Modeling. *J. Phys. Chem. A* **2007**, *111* (19), 4031−4042.
(70) Asatryan, R.; Rutz, L.; Bockhorn, H.; Bozzelli, J. Computational Thermochemistry and Kinetics for the HO_2 + CO Reaction. *International Workshop on Gas Kinetics*; Sonderforschungsbereich SFB 606: Karlsruhe, Germany, 2006.
(71) Mittal, G.; Sung, C.-J.; Fairweather, M.; Tomlin, A.; Griffiths, J.; Hughes, K. Significance of the HO_2 + CO reaction during the combustion of CO + H_2 mixtures at high pressures. *Proc. Combust. Inst.* **2007**, *31*, 419−427.
(72) Mueller, M. A.; Yetter, R. A.; Dryer, F. L. Flow reactor studies and kinetic modeling of the H_2/O_2/NOX and $CO/H_2O/O_2$/NOX reactions. *Int. J. Chem. Kinet.* **1999**, *31* (10), 705−724.
(73) Vardanyan, I. A.; Sachyan, G. A.; Nalbandyan, A. B. The rate constant of the reaction HO_2 + CO = CO_2 + OH. *Int. J. Chem. Kinet.* **1975**, *7* (1), 23−31.
(74) Carstensen, H.-H.; Dean, A. M.; Deutschmann, O. Rate constants for the H abstraction from alkanes (R-H) by $R'O_2$ radicals:

https://doi.org/10.1021/acsomega.3c07079
ACS Omega 2023, 8, 49098−49114

A systematic study on the impact of R and R′. *Proc. Combust. Inst.* **2007**, *31* (1), 149−157.
(75) Carstensen, H.-H.; Dean, A. M. Rate constants for the abstraction reactions RO_2+C_2H_6; R = H, CH_3, and C_2H_5. *Proc. Combust. Inst.* **2005**, *30* (1), 995−1003.
(76) Sirjean, B.; Dames, E.; Sheen, D.; You, X.; Sung, C.; Holley, A.; Egolfopoulos, F.; Wang, H.; Vasu, S.; Davidson, D.; et al. A high-temperature chemical kinetic model of *n*-alkane oxidation, JetSurF version 0.2. 2008, http://melchior.usc.edu/JetSurF/Version0_2/Index.html.
(77) Asatryan, R.; Hudzik, J.; Swihart, M. Intramolecular Catalytic Hydrogen Atom Transfer (CHAT). *J. Phys. Chem. A* **2023**. Submitted; jp-2023-06794r.
(78) Villano, S. M.; Huynh, L. K.; Carstensen, H.-H.; Dean, A. M. High-Pressure Rate Rules for Alkyl + O_2 Reactions. 1. The Dissociation, Concerted Elimination, and Isomerization Channels of the Alkyl Peroxy Radical. *J. Phys. Chem. A* **2011**, *115* (46), 13425−13442.
(79) Villano, S. M.; Huynh, L. K.; Carstensen, H.-H.; Dean, A. M. High-Pressure Rate Rules for Alkyl + O_2 Reactions. 2. The Isomerization, Cyclic Ether Formation, and β-Scission Reactions of Hydroperoxy Alkyl Radicals. *J. Phys. Chem. A* **2012**, *116* (21), 5068−5089.
(80) Burke, M. P.; Goldsmith, C. F.; Georgievskii, Y.; Klippenstein, S. J. Towards a quantitative understanding of the role of non-Boltzmann reactant distributions in low temperature oxidation. *Proc. Combust. Inst.* **2015**, *35* (1), 205−213.
(81) Goldsmith, C. F.; Burke, M. P.; Georgievskii, Y.; Klippenstein, S. J. Effect of non-thermal product energy distributions on ketohydroperoxide decomposition kinetics. *Proc. Combust. Inst.* **2015**, *35* (1), 283−290.
(82) Krep, L.; Kopp, W. A.; Kröger, L. C.; Döntgen, M.; Leonhard, K. Exploring the Chemistry of Low-Temperature Ignition by Pressure-Accelerated Dynamics. *ChemSystemsChem* **2020**, *2* (4), No. e1900043.
(83) Kelley, A. P.; Smallbone, A. J.; Zhu, D. L.; Law, C. K. Laminar flame speeds of C_5 to C_8 *n*-alkanes at elevated pressures: Experimental determination, fuel similarity, and stretch sensitivity. *Proc. Combust. Inst.* **2011**, *33* (1), 963−970.
(84) Ji, C.; Dames, E.; Wang, Y. L.; Wang, H.; Egolfopoulos, F. N. Propagation and extinction of premixed C_5-C_{12} *n*-alkane flames. *Combust. Flame* **2010**, *157* (2), 277−287.
(85) Dirrenberger, P.; Le Gall, H.; Bounaceur, R.; Glaude, P.-A.; Battin-Leclerc, F. Measurements of Laminar Burning Velocities above Atmospheric Pressure Using the Heat Flux Method-Application to the Case of *n*-Pentane. *Energy Fuels* **2015**, *29* (1), 398−404.

https://doi.org/10.1021/acsomega.3c07079
ACS Omega 2023, 8, 49098−49114